Computer-Aided Design 151 (2022) 103339

Contents lists available at ScienceDirect

Computer-Aided Design

journal homepage: www.elsevier.com/locate/cad

Geometric Moment-Dependent Global Sensitivity Analysis without Simulation Data: Application to Ship Hull Form Optimisation

Shahroz Khan [a,*], Panagiotis Kaklis [a], Andrea Serani [b], Matteo Diez [b]

[a] Department of Naval Architecture, Ocean and Marine Engineering, University of Strathclyde, Glasgow, United Kingdom
[b] CNR-INM, National Research Council-Institute of Marine Engineering, Rome, Italy

ARTICLE INFO

Article history:
Received 15 December 2021
Received in revised form 17 May 2022
Accepted 28 May 2022

Keywords:
Computer-aided design
Parametric sensitivity
Geometric moments
Moment invariant
Parametric design
Shape optimisation

ABSTRACT

In this work, we propose and test a method to expedite Global Sensitivity Analysis (GSA) in the context of shape optimisation of free-form shapes. To leverage the computational burden that is likely to occur in engineering problems, we construct a Shape-Signature-Vector (SSV) and propose to use it as a substitute for physics. SSV is composed of shapes' integral properties, in our case geometric moments and their invariants of varying order, and is used as quantity-of-interest (QoI) for prior estimation of parametric sensitivities. Opting for geometric moments is motivated by the fact that they are intrinsic properties of shapes' underlying geometry, and their evaluation is essential in many physical computations as they act as a medium for interoperability between geometry and physics.

The proposed approach has been validated in the area of computer-aided ship design with regard to the capability of global- and composite-SSV to reveal parametric sensitivities of different ship hulls for the wave-making resistance coefficient (C_w), which is a critical QoI towards improving ship's efficiency and thus decreasing emissions. More importantly, the longitudinal distribution of the volume below the ship's floating waterline, which is measurable via geometric moments, has an impact on C_w. Through extensive experimentation, we show a strong correlation between the sensitive parameters obtained with respect to SSV and those based on C_w. Consequently, we can estimate parameters' sensitivity with considerably reduced computational cost compared to when sensitivity analysis is performed with respect to C_w. Finally, two design spaces are constructed with sensitive parameters evaluated from SSV and C_w, and spaces' quality and richness are analysed in terms of their capability to provide an optimised solution.

1. Introduction

Computational design pipelines have become indispensable for handling various problems in science and engineering, which involves rapid exploration of parametric design spaces for global optima leading to shorter product development cycles. Physics-based simulation tools, such as Computational Fluid Dynamics (CFD), Computational Structural Dynamics (CSD), Computation Aeroacoustics (CAA), etc., are the key drivers of this exploration [1], which are continuously evolving to achieve a high level of fidelity. However, simultaneously they are becoming computationally intensive, requiring unaffordable computational resources even for a single simulation run [2]. As an example, a CFD-based statistically significant evaluation of ship performance in waves may require up to 1M CPU hours on HPC systems [3]. Consequently, the extensive use of these tools can be impractical for rich and vast design spaces, which are often incurred by design constraints to confine exploration to feasible designs [4]. A more critical bottleneck can be encountered if these spaces are high-dimensional, which is often favoured for maximal performance improvement [5], leading to the well-known curse of dimensionality and thus hampering the success of optimisation.

The existing techniques used to reduce the exorbitant computational costs mainly fall into two categories. One line of work focuses on developing computationally less demanding solvers [6,7] while the other leverages computational resources with data-driven approaches [8,9]. Recently, the most astounding results in reducing computational cost while maintaining the high approximation accuracy of designs' physics are achieved via data-driven approaches. These approaches can be broadly classified as dimensional reduction and surrogate modelling, employed to reduce the design space dimensionality and bypass designs' performance estimation with simulation tools, respectively [10]. For dimension reduction, there are well studied unsupervised (e.g., Principal Component Analysis (PCA) [4], auto-encoders [11], etc.) or supervised (e.g., Active Subspace Method (ASM) [12]),

* Correspondence to: University of Strathclyde, 16 Richmond St, Glasgow G1 1XQ, United Kingdom.
E-mail address: shahroz.khan@starth.ac.uk (S. Khan).

https://doi.org/10.1016/j.cad.2022.103339

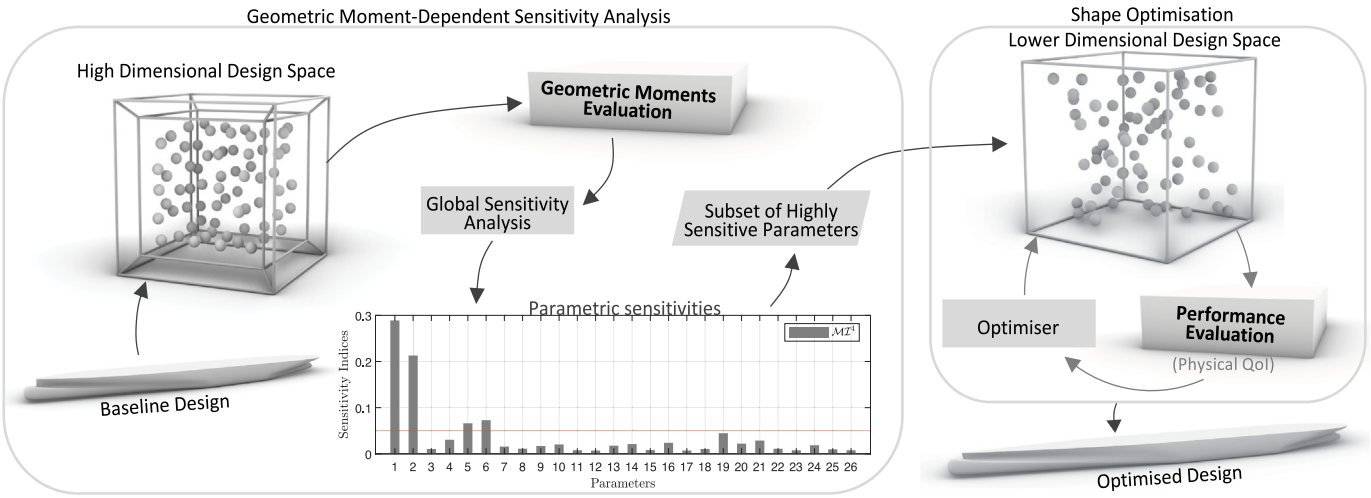

Fig. 1. Workflow of the proposed approach, which uses a shape-signature vector containing geometric moments of variant order for sensitivity analysis and design's physics for shape optimisation.

Sensitivity Analysis (SA), do or do not require data, correspondingly. Among these, PCA, auto-encoders, and ASM extract the latent features of the original design space to span a lower-dimensional subspace while materialising the maximum geometric variability. Contrary, SA is a down-selection process that screens out the parameters less sensitive (insensitive) to physics. As less sensitive parameters have a negligible effect on performance and they can be excluded to reduce the dimensionality of the design space [13].

The efficiency of both supervised and unsupervised approaches is manifested in various applications to mitigate the curse of dimensionality [11,14,15]. However, since unsupervised techniques do not require performance labels, their implementation can be less expensive than supervised methods. However, since there is no correlation between design and shape modification, these techniques can produce perfunctory subspaces, with the basis forming merely a new orientation of the design space without capturing any associated geometric features [4,15]. In contrast, SA implementation is more informed because, along with dimension reduction, its assessment is a meaningful prerequisite to reducing uncertainty and identifying the driving features of designs that account for the minimum or maximum variability in performance [10]. Consequently, SA may offer designers enhanced resource allocation from the preliminary design stage, thereby expediting product development. However, the implementation of SA can be computationally demanding, especially when the analytical solution is not available and running numerical simulations become mandatory.

To lessen the computational burden, surrogate models are often used to accelerate the SA as at the preliminary stage designers may not be interested in accurately estimating the performance [16]. Surrogate modelling is also a supervised learning approach, and despite the undoubted efficiency, their usage is often hindered by the availability of data, which is profound in engineering applications where data is the outcome of expensive physical simulations [2] and may exacerbate the entire design pipeline. Recently, to combat this insufficiency, these approaches have been revitalised via *scientific machine/deep learning*, such as Physics-Informed Neural Networks (PINN) [9]. PINNs are trained to integrate differential equations modelling the physics along with a moderate amount of data from simulations or experiments to approximate the underlying Partial Differential Equations (PDE) solution. In fact, if the PDE problem is well-defined along with appropriate initial and boundary conditions, then PINN can identify the unique solution without any simulation data [2]. Their potential has been exploited in fluid mechanics [9], solid mechanics [17] and dynamical systems [18].

Motivated by these approaches, we aim to address the aforementioned challenges associated with SA by offloading the evaluation of parametric sensitivities from physical quantities to relatively inexpensive quantities compared to physical ones but provide important clues about the form distribution and validity of the design. More specifically, it is well known that shape's integral properties, such as geometric moments and their invariants [6,19] serve as a geometric foundation for different designs' physical analyses. Like physics, they rely strongly on design's geometry, but their evaluation is substantially less expensive. Therefore, we propose a geometric moment-dependent SA approach that harnesses the geometric variation of designs in a design space using geometric moments as a geometrical Quantity of Interest (QoI) to measure parametric sensitivities. These results can serve as a prior estimation of parametric sensitivities and use to construct a design space of lower dimension with only a subset of highly/strongly sensitive parameters for shape optimisation performed against physical QoI. This approach can significantly reduce the computational time because, typically, sensitivities are learnt directly with physical QoI, which can add a heavy computational burden on the entire design process as one has to perform computationally intensive physical simulations for both SA and shape optimisation. Fig. 1 shows the systematic workflow of the proposed approach, which uses geometric moments for SA and design's physics for shape optimisation. The selection of geometric moments for SA in our work is motivated by the following fundamental insights:

1. Geometric moments of a shape are intrinsic properties of its underlying geometry and act as a unifying medium between geometry and its physical evaluation [20,21].
2. Physical analysis requires the evaluation of such integral properties of the geometry such as the stiffness and mass matrices, and moments of a domain are sufficient to ensure accurate integration of a large class of integrands [6,22].
3. Like physics, geometric moments also act as a compact shape signature or descriptor to a specific design falling in a specific category, which facilitates various shape processing tasks [23–25].

In this work, we show through extensive experiments the competitive performance of the geometric moments for making an informed decision on the sensitivity of parameters without

performing computationally intensive physical simulations. The results of SA via geometric moments permit to categorised a prior the design parameters as *strongly sensitive*, *moderately sensitive*, *weakly sensitive*, and *insensitive*. According to Sheikholeslami et al. [16] and Klepper [26], when such categorisation of parameters is available, then computationally efficient SA with physics can be performed for each category. As explained earlier in this section, different physical analyses have a dependence on shape integral properties such as geometric moments, but during any design process, there are many physical criteria (varying from application to application) that have to be investigated and may not be dependent on geometric moments. *Thus, the use of moments does not aim to eliminate the need to perform SA with respect to physics but rather to support the designer for a prior check regarding the sensitivity of parameters for those physical quantities that are computationally expensive and share relevance with geometric moments*. Therefore, we restrict our aim to exploring the capability of these geometric moments in the context of ship-hull design, namely, with regard to their capability to reveal the sensitivity of its parameters for the wave-making resistance coefficient (C_w), which is one of the significant components of total ship's resistance and a critical design criterion.

Wave-making is caused when an object moves on or near the free surface of the water. The waves are generated from the variation of pressure over the wetted surface of the ship and carried behind it in the form of the so-called Kelvin wave pattern through a mechanism that is due to the kinematic and dynamic conditions satisfied on the free surface of the ocean. The importance of C_w reduction at the preliminary design stage, its effect on hull geometry and its connection with geometric moments will be discussed and formulated in Section 4.1. To experimentally demonstrate the effectiveness of geometric moments, we used two ship hulls parameterised with 26 and 27 parameters using two different techniques based on *Procedural Deformation* (PD) [27] and *Global Modification Function* (GMF) [4], respectively. The former parameterises a hull geometry constructed using the NURBS (non-uniform rational B-splines) representation and parameters directly associated with the hull's key features. In contrast, the latter is defined directly on a design grid and creates a global surface deformation. For the hull parameterised with PD, its C_w is evaluated using an inviscid BEM (Boundary Element Method) isogeometric solver [7]. For the GMF-based hull, C_w is obtained with a method based on the linear potential flow theory as well [28]. Geometric moments for both hulls are evaluated via the divergence theorem [29], which is applied on the triangulated mesh surfaces of the hull.

To commence SA, we first construct the so-called *Shape-Signature Vector* (SSV), which acts as a unique descriptor for the shape and contains all the geometric moments up to a certain order. To better correspond to C_w, all the moments in this vector are formulated to be invariant to translation and scaling. A global variance-based SA [30] is performed concerning SSV and C_w. Here, the former is purely a vector quantity containing the moment of various orders, while the latter is a scalar one but computationally expensive to evaluate. Therefore, learning sensitivity to SSV requires implementing a multivariate output SA technique, such as covariance decomposition [31], which provides generalised sensitivity indices of design parameters to all moments in SSV. Afterwards, a series of experimentations are performed to identify a common set of sensitive parameters between SSV and C_w. Furthermore, the higher the order of SSV is, the better it can describe the shape, and as a result, its parametric sensitivity better correlates with C_w. However, evaluation of higher-order moments can be prone to numerical noise. Therefore, following various other applications of moments in literature [20,32] we restrict our analysis to geometric moments up to fourth-order. We also study the local effect of geometric moments evaluated after segmenting the hull shape to compensate for this. To further demonstrate the effectiveness of geometric moments, for each test case, two shape optimisations are performed in the design spaces constructed with parameters sensitive to SSV and C_w. Their results are compared to optimal design obtained when optimisation is performed within the actual high-dimensional design space.

The remainder of this paper is organised as follows: Section 2 gives an overview of the relevant works proposed for computationally effective SA. Section 3 discusses the problem formulation, evaluation of geometric moments and SA for problems with univariate and multivariate outputs. A detailed discussion on the relevance of geometric moments with C_w, along with the description of the test cases, is given in Section 4. The numerical results of the proposed technique are provided in Section 5. Concluding remarks and plans for future work are presented in Section 6.

2. Related works

As stated in the introduction, the work aims not to propose a new SA approach; instead, it intends to use computationally efficient and physically linked geometric functionals to expedite SA, especially at the preliminary design stage, where the decision on the selection of effective design parameters is critical. Before delving into the core formulation of the proposed approach, we first briefly review previous work in SA while restricting our exposition to work dealing with reducing their computational cost. We also briefly discuss the application of geometric moments in design and analysis.

2.1. Sensitivity analysis (SA)

SA is widely used in various applications for different purposes, but as stated in [33], one of its primary goals is to reduce the dimensionality of the design space by screening out the less sensitive parameters to designs' performance. It should be noted that there are two types of approaches in the field of parametric SA, namely the local (LSA) and global SA (GSA). LSA is usually derivative-based [34,35], in which the change in QoI is evaluated against the variation of a single parameter. LSA investigates how a small perturbation near an input space value influences the value of QoI. On the contrary, in GSA, all parameters are varied simultaneously, and sensitivity is assessed over the entire range of each design parameter constructing the design space [16,34]. In complex engineering problems, the influence of a design parameter may vary drastically as the remaining parameters change. Thus, it could be inadequate to evaluate the impact of a parameter on the QoI with the other parameters being kept constant. Accordingly, selecting significant parameters for shape optimisation based on their GSA is more appropriate in real-world applications [36] and used in the present work.

The analytical implementation of GSA can often be tricky as it requires solving high-dimensional integrals. In this case, one has to appeal to sampling methods, such as Monte Carlo sampling (MCS) [16]. However, MCS is susceptible to slow convergence for stable results, as it requires the evaluation of a sufficiently large number of samples via computationally intensive physical simulations. Although a slightly better convergence rate can be obtained with quasi-Monte Carlo (Q-MC) or Latin-Hypercube (LH) methods, which are based on uniformly distributed design sequences, their advantage downgrade considerably in high-dimensional design spaces [16]. A sequential strategy, namely progressive Latin hypercube sampling (PLHS), was proposed by Sheikholeslami and Razavi [33]. As implied by its label, PLHS searches the design in the class of Latin hypercube and uses a

criterion of space-filling to uniformly distribute the designs in a sub-set of sliced design spaces. Similar to [33], Wu [37] also utilised space-filling to propose a SA, which initially commences with samples obtained using the max–min principle of Latin hypercube, whose spread was improved by maximising a Euclidean distance with a coordination sorting algorithm. Gong et al. [38] compared different baseline sampling approaches, such as good lattice points, symmetric Latin hypercube uniformity, Ranked Gram–Schmidt and Quasi-Monte-Carlo, against uniformity scores and found out that a better convergence can be achieved with the first two approaches. Recently, Khan and Kaklis [10] proposed a Dynamic Sampling Strategy (DSS), which, along with space-filling, involves criteria of non-collapsing and repulsion. This method progressively increases the number of samples in each iteration; the non-collapsing maintains the diversity while repulsion helps create designs different from previously sampled ones in each iteration. DSS is proven to approximate a solution closer to the analytical one with small sample size and, therefore, used in the present work.

As mentioned earlier, surrogate models such as non-parametric regression [39], polynomial chaos expansions [40], support vector machines [41], low-rank tensor approximations [42], Gaussian processes [8], and other Kriging methods [43] are also widely used for revealing parametric sensitivities with respect to costly physical quantities. Apart from the traditional surrogate modelling approaches, deep learning approaches [44] have recently gained attention specifically for quantifying key resource uncertainty in the system. Despite their proven efficiency, the sensitivity of parameters evaluated with these methods heavily depends on the accuracy of the surrogate models [8,16].

Along with using retrofitted versions of the sampling methods to improve convergence and surrogate models to bypass expensive physics evaluation, few attempts have been made to ease the computational burden in the context of reducing the dimensions of a high-dimensional problem before performing SA. For instance, Pronzato [45] used a Bayesian Linear Model constructed through a particular Karhunen–Loéve expansion to estimate Sobol's indices at a reduced computational cost. Furthermore, Sheikholeslami et al. [16] utilised a clustering-based strategy to ease the computational burden of implementing typical SA on high-dimensional design problems. Masood et al. [8] performed the eigendecomposition of the original design space using PCA and then proposed a method to drive the sensitivity of actual parameters from their lower-order projection. This method reduces the number of samples required to evaluate the robust sensitivity indices.

Apart from the high computational cost, another significant but often neglected challenge SA has to deal with is related to the fact that the sensitivity of parameters varies locally within the design space, meaning a parameter can be sensitive in some local regions of the design space but become insensitive in others. Such behaviour makes SA vulnerable to instabilities even with slight perturbation in the parametric ranges of the design space. Consequently, SA should be performed with caution, especially at the preliminary design stage. At this stage, the design problem is not well established, and designers are not aware of the appropriate parametric ranges for performing a reliable sensitivity study. SA within a non-viable design space can be dismayed, eliminating essential parameters from the design study. To tackle this problem, approaches like regional SA [46] and intra-sensitivity [10] have been proposed in the literature to evaluate the behaviour of parametric sensitivity in local regions of the design space and to identify parameters whose perturbation in the range generates the most considerable inconsistency in the sensitivity of other parameters, respectively. Although these techniques can provide substantial aid to designers for reliable sensitivity studies, they are computationally demanding because of the extraction of the local behaviour of parametric sensitivities. Therefore, in this work, we appeal to a different direction to support the sensitivity study of design problems using quantities like geometric moment invariants, which, compared to physical criteria, are time inexpensive even for complex free-form or organic shapes but provide important clues regarding the physics. This work performs an extensive experimental study to prove that geometric moments can ease the designer for estimating parameters' sensitivity at the initial design stage.

2.2. Geometric moments in design and analysis

From a geometric point of view, these moments are typically used to evaluate the overall volume enclosed by the shape, its centre of mass, and moment of inertia. Geometric moments are used over a wide spectrum of applications ranging from probability and statistics to signal processing, computing tomography [47], object recognition [25], shape retrieval [24], rigid body transformation [23], feature extraction [48] etc. In physical analyses, they are used for governing equation of motions for flows around a body [20], integrating accurately implicit functions [22], modelling nonlinear material properties in the cut-cell method [49], simplifying history-dependent material modelling in the case of crack propagation [50], and material field modelling to develop an integral representation for fields that supports a wide range heterogeneous data [21]. Recently, meshfree methods have also been developed [6,51,52], which use moments to generate quadrature rules for the geometric domain to aid the interoperability between CAD representation and its physics.

Similar to the present work, Taber et al. [6] used a moment-vector for composing components of moments of a different order; however, there is a slight difference in their construction and the number of moments they contain. A new integration technique called Shape Aware Quadratures (SAQ) was proposed by Vaidyanathan, and Vadim [51] to efficiently integrate arbitrary integrable functions over arbitrary 2D/3D domains even in the presence of small features. It uses different derivative-based shape sensitivities of first and second-order to construct shape correction factors used in the moment-fitting equations. These shape correction factors ensure that the quadrature rule determined by the moment-fitting equations is aware of the shape of the integration domain, especially associated with the small features. Christian et al. [52] proposed a new type of analysis pipeline, eXtended Finite Element Method (XFEM), mainly to support smooth interoperability between CAD and physical simulation during shape optimisation. The core of their contribution lies in using a moment-fitting technique to compute on-the-fly a modified set of quadrature rules that accurately handle integration over curved domains of varying shape and size, bounded by NURBS and planar patches, and evaluate shape derivatives with respect to these rules to quantify the shape sensitivities caused on the volume integral with the change of the design parameters. The derivative-based shape sensitivities evaluated in [51,52] are usually referred to as local sensitivities [34,35], which enables identifying the local influence of a single parameter on the QoI. As explained earlier, in this work, we use GSA, which provides a holistic view of the influence of all design parameters on the QoI in question.

3. Geometric moment-based sensitivity analysis

This section provides an in-depth description of the proposed approach, including the general assumptions, mathematical formulation of geometric moments and their invariants and a brief overview of SA for univariate and multivariate outputs models.

3.1. Problem formulation

Let a geometric design $\mathcal{G}$ be parameterised with a set of n continuous design parameters $\mathbf{t} = \{t_i, i = 1, 2, \ldots, n\} \in \mathcal{X} \subseteq \mathbb{R}^n$. Here $\mathcal{X}$ is the n-dimensional solution/design space, bounded by lower $\mathbf{t}^l$ and upper $\mathbf{t}^u$ limits of the associated parameters (i.e., $\mathcal{X} := \{t_i^l \leq t_i \leq t_i^u, \forall i \in \{1, 2, \ldots n\}\}$). Moreover, all the elements of $\mathbf{t}$ are assumed to be statistically independent from each other, i.e., $p_{\mathbf{t}}(\mathbf{t}) = \prod_{i=1}^{n} p_{t_i}(t_i)$, where $p_{\mathbf{t}}(\mathbf{t}) : \mathbb{R}^n \to \mathbb{R}$ represents the Probability Density Function (PDF) of $\mathbf{t}$ and $p_{t_i}(t_i)$ is the marginal PDF of t_i. Now, the objective of the present work is to assess the sensitivity indices, $\mathbf{SI} = \{SI_1, SI_2, \ldots, SI_n\}$, of each element of $\mathbf{t}$ with respect to geometrical QoI, such as geometric moments of $\mathcal{G}$. Therefore, we assume to possess a shape-signature vector, $\mathcal{MI}^s$, which contains all the geometric moments from 0th to sth order. Construction of $\mathcal{MI}^s$ will be discussed in detail in the subsequent subsections. Once the SA is performed, the aim is to find a subset $\mathbf{t}_{\mathcal{MI}}$ of m highly sensitive parameters whose sensitivity index is greater than a threshold, ϵ, where m is favourable to be less than n. The subset of m parameters forms a design space $\mathcal{X}_{\mathcal{MI}}$ of reduced dimension, which is exploited to expedite the shape optimisation carried out directly with a physical QoI; represented as $y = g(\mathbf{t}) : \mathcal{X} \subseteq \mathbb{R}^n \to \mathbb{R}$. In conclusion, the overall problem can be stated as follows:

Sensitivity:

$$\begin{aligned} \text{Find } \mathbf{t}_{\mathcal{MI}} \subseteq \mathbf{t} \quad & \text{sensitive w.r.t. } \mathcal{MI}^s \\ \text{where} \quad & \mathbf{t} \in \mathcal{X} \subseteq \mathbb{R}^n \\ \text{Construct } \mathcal{X}_{\mathcal{MI}} \quad & \text{such that} \\ & \mathbf{t}_{\mathcal{MI}} \in \mathcal{X}_{\mathcal{MI}} \subseteq \mathbb{R}^m \\ & m < n \end{aligned} \tag{1}$$

Optimisation:

$$\begin{aligned} \text{Find } \mathbf{t}^*_{\mathcal{MI}} \in \mathbb{R}^m \quad & \text{such that} \\ g(\mathbf{t}^*_{\mathcal{MI}}) = & \min_{\mathbf{t}_{\mathcal{MI}} \in \mathcal{X}_{\mathcal{MI}}} g(\mathbf{t}^*_{\mathcal{MI}}) \end{aligned}$$

3.2. Geometric moments

We shall use moments for quantifying the shape of an object (design, in the so-far terminology) $\mathcal{G}$ of finite extent, defined by the following formula:

$$M^{p,q,r}(\mathcal{G}) = \int_{-\infty}^{+\infty} \int_{-\infty}^{+\infty} \int_{-\infty}^{+\infty} x^p\, y^q\, z^r\, \rho(x, y, z)\, \mathrm{d}x\mathrm{d}y\mathrm{d}z, \quad \text{with} \quad p, q, r \in \{0, 1, 2, \ldots\}, \tag{2}$$

which gives the sth-order geometric moment of $\mathcal{G}$, where $s = p + q + r$ and $\rho(x, y, z) = 1/0$ for $(x, y, z) \in / \notin \mathcal{G}$, respectively. Given a non-negative integer s, the vector $\mathbf{M}^s$ will contain $(s+1)(s+2)/2$ moments $M^{p,q,r}(\mathcal{G})$ such that $p + q + r = s$. The ideal order of $\mathbf{M}$ will result in a vector containing geometric moments capturing not only global features of the shape but also the local features. For instance, moment of $(s = 2)$th-order contains

$$\mathbf{M}^2 = \begin{bmatrix} M^{2,0,0}(\mathcal{G}) & M^{0,2,0}(\mathcal{G}) & M^{0,0,2}(\mathcal{G}) & M^{1,1,0}(\mathcal{G}) & M^{1,0,1}(\mathcal{G}) & M^{0,1,1}(\mathcal{G}) \end{bmatrix}. \tag{3}$$

As pointed out in [6], moments can be thought of as projections (with respect to L^2 inner product) of ρ onto any polynomial basis, such as monomials, Legendre polynomials, etc. In Mathematical Analysis, the classical moment problem, which has been treated by various famous mathematicians such as Markov in 1883 and Stieltjes in his famous 1894 paper on: "Recherchers sur les fractions continues", can be simply stated as follows: *Recover a function $f(x)$ given its moments $M^p = \int x^p f(x) dx$, $p = 0, 1, \ldots$.* In all these guises, the moment problem is recognised as a notoriously difficult inverse problem, often leading to the solution of very ill-posed systems of equations that usually do not have a unique solution [47].

In Eq. (2), if $\rho(x, y, z)$ represents the volume density then the zero- and first-order moments, $M^{0,0,0}(\mathcal{G})$, $M^{1,0,0}(\mathcal{G})$, $M^{0,1,0}(\mathcal{G})$, and $M^{0,0,1}(\mathcal{G})$, are widely used in computer graphics, CAD and engineering for computing the object volume, $\mathcal{V} = M^{0,0,0}(\mathcal{G})$, and the coordinates of the centre-of-volume:

$$\mathbf{c}(\mathcal{G}) = \begin{bmatrix} C_x \\ C_y \\ C_z \end{bmatrix} = \begin{bmatrix} \frac{M^{1,0,0}(\mathcal{G})}{M^{0,0,0}(\mathcal{G})} \\ \frac{M^{0,1,0}(\mathcal{G})}{M^{0,0,0}(\mathcal{G})} \\ \frac{M^{0,0,1}(\mathcal{G})}{M^{0,0,0}(\mathcal{G})} \end{bmatrix}. \tag{4}$$

If $\rho(x, y, z)$ is the PDF of a continuous random variable, then $\mathbf{M}^0$, $\mathbf{M}^1$, $\mathbf{M}^2$, $\mathbf{M}^3$ and $\mathbf{M}^4$, represent the total density, mean, variance, skewness and kurtosis of the random variable, respectively. Moreover, the moments of second-order can be organised in a second rank tensor, the moment of inertia tensor (MoI), which is represented as follows:

$$\text{MoI} = \begin{bmatrix} M^{0,2,0}(\mathcal{G}) + M^{0,0,2}(\mathcal{G}) & -M^{1,1,0}(\mathcal{G}) & -M^{1,0,1}(\mathcal{G}) \\ -M^{1,1,0}(\mathcal{G}) & M^{2,0,0}(\mathcal{G}) + M^{0,0,2}(\mathcal{G}) & -M^{0,1,1}(\mathcal{G}) \\ -M^{1,0,1}(\mathcal{G}) & -M^{0,1,1}(\mathcal{G}) & M^{2,0,0}(\mathcal{G}) + M^{0,2,0}(\mathcal{G}) \end{bmatrix}. \tag{5}$$

As mentioned earlier, the more moments we use, the better we capture the shape's intrinsic features. Our moment-driven SSV is represented by $\mathcal{M}^s = \left[\mathbf{M}^0, \mathbf{M}^1, \mathbf{M}^2, \ldots, \mathbf{M}^s\right]$, where s is appropriately large to cover the shapes of interest [23]. Theoretically, s ranges from 0 to ∞, though there exist object classes for which s is finite when, e.g., dealing with the class of the so-called quadrature domains in the complex plane [53] or when approximating convex bodies using Legendre moments [54].

There exists a variety of methods available in the literature for computing geometric moments, which use either lower-order approximating mesh [55] or high-order surface [19] representations, such as B-splines and NURBS, of $\mathcal{G}$. The most commonly used method is Gauss's divergence theorem [29], which evaluates geometric moments by converting volume integrals to integrals over the surface bounding the volume. In the Appendix, we summarise the evaluation of geometric moments using the divergence theorem for a triangulation $S = \bigcup_{i=1}^{N} T_i$ approximating the surface bounding $\mathcal{G}$, where N is the total of triangular elements T.

3.2.1. Geometric moment invariants

The moments in $\mathbf{M}^s$ are variant with respect to rigid and non-rigid transformations, such as translation, rotation and scaling [56]. However, most physical quantities are invariant to either all or some of these transformations. For instance, evaluating C_w for the ship is invariant to translation and scaling if assessed at a certain Froude number. Therefore, to measure the sensitivity of these parameters with respect to the geometry, the invariant of these geometric moments with respect to translation and scaling has to be secured. A description of geometric moment invariants with respect to translation and scaling presented in this section and their other invariants can be found in [56].

If Eq. (2) is applied for $\mathcal{G}$, while placing it at its centroid, $\mathbf{c}(\mathcal{G}) = (C_x, C_y, C_z)$, then we get the so called *central geometric moment* of sth-order, which is invariant to translation and is expressed as:

$$\mu^{p,q,r}(\mathcal{G}) = \int_{-\infty}^{+\infty} \int_{-\infty}^{+\infty} \int_{-\infty}^{+\infty} (x - C_x)^p\, (y - C_y)^q\, (z - C_z)^r \times \rho(x, y, z)\, \mathrm{d}x\mathrm{d}y\mathrm{d}z. \tag{6}$$

It is noteworthy that as $\mathcal{G}$ is placed at its centroid; therefore the first-order moment is zero, i.e., $[\mu^{1,0,0}, \mu^{0,1,0}, \mu^{0,0,1}] = 0$. To achieve invariance of $\mu^{p,q,r}$ to scaling we assume that $\mathcal{G}$ is uniformly scaled by a factor λ, which gives

$$\hat{\mu}^{p,q,r}(\hat{\mathcal{G}}) = \lambda^{p+q+r+3}\mu^{p,q,r}(\mathcal{G}). \tag{7}$$

Then, one can easily conclude that

$$MI^{p,q,r} = \frac{\mu^{p,q,r}}{(\mu^{0,0,0})^{1+(p+q+r)/3}} \tag{8}$$

is an invariant moment form for $\mathcal{G}$ under uniform scaling and translation [56]. For any non-negative integer, s, the moment invariant vector, $\mathbf{MI}^s$ contains all the moments invariant to translation and scaling such that $p+q+r = s$. By definition this invariance satisfies $MI^{0,0,0} = 1$ and $\mathbf{MI}^1 = \left[MI^{1,0,0}, MI^{0,1,0}, MI^{0,0,1}, MI^{1,1,0}, MI^{1,0,1}, MI^{0,1,1}\right] = 0$. As $M^{0,0,0}$ represents the volume of $\mathcal{G}$, which is intrinsically invariant to translation; therefore, the invariant SSV, $\mathcal{MI}^s$, contains $M^{0,0,0}$ instead of $MI^{0,0,0}$ (i.e., $\mathcal{MI}^s = \left[M^{0,0,0}, \mathbf{MI}^2, \mathbf{MI}^3, \ldots, \mathbf{MI}^s\right]$).

3.3. Global sensitivity analysis

In GSA, variability of QoI is measured when all parameters vary over the entire design space. This allows users to evaluate the relative contribution of each parameter to QoI's output variation, which is the focus of the present study. Different sensitivity analyses have been proposed in the literature, such as variance-based (or Sobol's method), density-based sensitivity, elementary effects test (or Morris method), etc. Interested readers can refer to [30] for a detailed overview of these techniques. Among these methods, variance-based probabilistic methods like Sobol's analysis [57] is suitable for complex nonlinear and non-additive models; therefore, it is well received in different design applications and thus used in the current study. This method investigates how much of the overall variance of QoI is achieved due to the variability of a collection of design parameters. This variance is usually measured with *First-order indices* (or *main effects*) or *total-order indices* (or *total effects*). The former quantifies the direct contribution to QoI variance from an individual parameter over the entire design space. The latter approximates the overall contribution of a parameter considering its direct effect and interactions with all the other design parameters.

3.3.1. Sobol's sensitivity analysis

Sobol's analysis is often classified as a variance-based model-independent method, which is based on the variance decomposition and can handle the underlying non-linearity of QoI under consideration. Under the probabilistic interpretation of elements of $\mathbf{t}$, Y is the output of g with mean ($\mathbb{E}(Y)$) and variance ($V(Y)$). Consider $g(t_1, t_2, \ldots, t_n)$ to be square integrable over $\mathcal{X} \subseteq \mathbb{R}^n$ with Lebesgue measure $\mathrm{d}\mathbf{t} = \mathrm{d}t_1 \ldots \mathrm{d}t_n$. The Sobol's SA is based on a decomposition of the model into summands of functions of increasing dimensionality referred to as ANOVA (functional ANalysis Of VAriance) or *Hoeffding–Sobol* decomposition [57], that can be written as

$$g(\mathbf{t}) = g_0 + \sum_{s=1}^{n} \sum_{i_1<\cdots<i_s} \left(t_{i_1}, \ldots t_{i_s}\right), \tag{9}$$

where g_0 is the expectation (mean) of Y defined as

$$g_0 = \mathbb{E}(Y) = \int_{-\infty}^{\infty} \cdots \int_{-\infty}^{\infty} g(t_1, \ldots, t_n) \prod_{k=1}^{n} p_{t_k}(t_k) dt_k, \tag{10}$$

and $g_{i_1,\ldots,i_s}(t_{i_1}, \ldots t_{i_s})$ satisfy the unicity condition

$$\int g_{i_1,\ldots,i_s}(t_{i_1}, \ldots t_{i_s}) p_{t_{i_1,\ldots,i_2}}(t_{i_1}, \ldots, t_{i_s}) dt_{i_1} \ldots dt_{i_s} = 0,$$

$$s = 1, 2, \ldots, n. \tag{11}$$

The interior sum in Eq. (9) can be extended over all different groups of indices $i_1, i_2, \ldots, i_s$ such that $1 \le i_1 < i_2 < \cdots < i_s \le n$. With this condition, Eq. (9) can be expanded as

$$g(t_1, \ldots, t_n) = g_0 + \sum_{i=1}^{n} g_i(t_i) + \sum_{i=1}^{n} \sum_{j=i+1}^{n} g_{ij}(t_i, t_j) + \cdots + g_{1,\ldots,n}(t_1, \ldots, t_n). \tag{12}$$

Eq. (12) consists of 2^n terms with each term is assumed to be squared integral over $\mathcal{X}$ with zero average. The terms $g_i(t_i)$, $1 \le i \le n$, are functions of a single variable and are the so-called first-order indices (or main effect). Each of them represents the variation in Y due to the change in t_i. The functions of more than one variable, $g_{ij}(t_i, t_j)$, $1 \le i \le j \le n$, are called *interactions* and represent the variation in Y not accounted when t_i and t_j vary individually. With the condition in Eq. (11), all the terms in Eq. (12) are naturally orthogonal and can be expressed as integrals of $g(t)$ as

$$g_i(t_i) = \int_{-\infty}^{\infty} \cdots \int_{-\infty}^{\infty} g(t_1, \ldots, t_n) \prod_{k=1, k\neq i}^{n} p_{t_i}(t_i) dt_1 \ldots dt_n - g_0 = \mathbb{E}_{\mathbf{t}_{\sim i}}(Y|t_i) - g_0, \tag{13a}$$

$$g_{ij}(t_i, t_j) = \int_{-\infty}^{\infty} \cdots \int_{-\infty}^{\infty} g(t_1, \ldots, t_n) \prod_{k=1, k\neq ij}^{n} p_{t_i}(t_i) dt_1 \ldots dt_n - g_i - g_j - g_0 = \mathbb{E}_{\mathbf{t}_{\sim ij}}(Y|t_i, t_j) - g_i - g_j - g_0. \tag{13b}$$

In the similar way, Eq. (13) continues for the higher-orders. Here, $\mathbb{E}_{\mathbf{t}_{\sim i}}(\cdot)$ is the mean of Y taken over all possible values of $\mathbf{t}$ when t_i is fixed through its full distribution range, whereas $\mathbb{E}_{\mathbf{t}_{\sim ij}}(\cdot)$ is also the mean of Y but evaluated when both t_i and t_j are fixed.

With the hypothesis that all the input parameters are independent of each other, the variance of the output ($V(Y)$) can be also be decomposed into $2^n - 1$ partial variances of increasing orders as [58]

$$V(Y) = \sum_{i}^{n} V_i + \sum_{i} \sum_{j=i+1}^{n} V_{ij} + \cdots + V_{12\ldots n} \tag{14}$$

where

$$V_i = V(g_i(t_i)) = V_{t_i}\left(\mathbb{E}_{\mathbf{t}_{\sim i}}(Y|t_i)\right), \tag{15a}$$

$$V_{ij} = V\left(g_{ij}(t_i, t_j)\right) = V_{t_i,t_j}\left(\mathbb{E}_{\mathbf{t}_{\sim ij}}(Y|t_i, t_j)\right) - V_{t_i}\left(\mathbb{E}_{\mathbf{t}_{\sim i}}(Y|t_i)\right) - V_{t_j}\left(\mathbb{E}_{\mathbf{t}_{\sim j}}(Y|t_j)\right). \tag{15b}$$

Herein, $V_{t_i}(\cdot)$ and $V_{t_j}(\cdot)$ is the variance over all possible values of t_i and t_j, respectively. The contribution of individual design parameter's variance to the total output variance can be evaluated with the above relation. Therefore, by the dividing Eq. (13) with the total variance $V(Y)$ of Y one could determine the first and second-order sensitivity index of t_i as

$$SI_i = \frac{V_i}{V(Y)} = \frac{V_{t_i}\left(\mathbb{E}_{\mathbf{t}_{\sim i}}(Y|t_i)\right)}{V(Y)}, \tag{16a}$$

$$SI_{ij} = \frac{V_{ij}}{V(Y)} = \frac{V_{t_i,t_j}\left(\mathbb{E}_{\mathbf{t}_{\sim ij}}(Y|t_i, t_j)\right) - V_{t_i}\left(\mathbb{E}_{\mathbf{t}_{\sim i}}(Y|t_i)\right) - V_{t_j}\left(\mathbb{E}_{\mathbf{t}_{\sim j}}(Y|t_j)\right)}{V(Y)}. \tag{16b}$$

Likewise, indices of the sth-order can be defined as

$$SI_{i_1,i_2,\ldots,i_s} = \frac{V_{i_1,i_2,\ldots,i_s}}{V(Y)}. \tag{16c}$$

SI_i is the main effect index of t_i and can also be referred to as the average reduction of the total variance of Y when t_i is fixed over its full distribution range. Another well known variance-based sensitivity measure is the total effect sensitivity index [58], which can be derived as

$$SI_{Ti} = \frac{\mathbb{E}_{\mathbf{t}\sim i}\left(V_{t_i}\left(Y|\mathbf{t}_{\sim i}\right)\right)}{V(Y)} = 1 - \frac{V_{\mathbf{t}\sim i}\left(\mathbb{E}_{t_i}\left(Y|\mathbf{t}_{\sim i}\right)\right)}{V(Y)}. \tag{17}$$

Here, SI_{Ti} is the total sensitivity index for t_i and $\mathbb{E}_{\mathbf{t}\sim i}\left(V_{t_i}\left(Y|\mathbf{t}_{\sim i}\right)\right)$ is the expected reduction in variance that is obtained if all, but t_i, parameters are fixed. The lower value of SI_{Ti} represents t_i which is less significant. Furthermore, the indices in Eq. (16) satisfy $\sum_i SI_i + \sum_i \sum_{j>i} SI_{ij} + \cdots + SI_{12\ldots n} = 1$ and sum of the indices in Eq. (16a) is greater than or equal to one. In this analysis, if $SI_i = SI_{Ti}$ then there is no interaction effect between t_i and other elements of $\mathbf{t}$ and model is additive, which, based on the assumption of orthogonality of input parameters. If a model is not additive then Sobol's indices can also be used for identifying the effective dimensions [13].

In summary, SI_i as the main effect measures the fractional contribution of a single parameter to the output variance. SI_{ij} are used to measure the fractional contribution of parameter interactions to the output variance. The total effect, SI_{Ti}, is more adequate as its evaluation takes into account the main, second-order, and higher-order effects over the entire range of $\mathcal{X}$ [58]. Therefore, in this work, we focus on evaluating SI_{Ti} of parameters with respect to $\mathcal{MI}^s$. However, as shown above, the analytical evaluation of SI_{Ti} requires solving high-dimensional integrals; therefore, as explained in Section 2, sampling methods are used.

3.4. Sensitivity analysis of multivariate output

$\mathcal{MI}^s$ of sth-order is a vector quantity composed of multiple moments invariant vector terms. For instance, $\mathcal{MI}^2$ is composed of one zeroth-order and six second-order moment invariants, which create a problem with the multivariate output. The typical Sobol decomposition is obtained for each component of the model output, leading to many sensitivity measures for each output variable. These sensitivities can be redundant if the correlation in the model output is essential, leading to difficulties interpreting these results. To deal with this problem, two different alternatives have been proposed in the literature for multivariate output, referred to as output decomposition [59] and covariance decomposition [31] approaches.

3.4.1. Output decomposition method

The output decomposition method was initially proposed by Campbell et al. [59] and is based on the eigendecomposition of a set of output variables into a lower-dimensional representation. Therefore, it is primarily suitable for problems involving time series output data in which the dimensionality of model output is extensively high. Since $\mathcal{MI}^s$ is the QoI in the present case, we assume that the elements of the $\mathcal{MI}^s$ form a moment space from which a dataset $\mathbb{MI}$ consisting of N' samples is constructed as

$$\mathbb{MI} = \begin{bmatrix} \mathcal{MI}^s_1 \\ \mathcal{MI}^s_2 \\ \vdots \\ \mathcal{MI}^s_{N'} \end{bmatrix} = \begin{bmatrix} \mathbf{MI}^0 & \mathbf{MI}^2_1 & \mathbf{MI}^3_1 & \ldots & \mathbf{MI}^s_1 \\ \mathbf{MI}^0_2 & \mathbf{MI}^2_2 & \mathbf{MI}^3_2 & \ldots & \mathbf{MI}^s_2 \\ \vdots & \vdots & \vdots & \ddots & \vdots \\ \mathbf{MI}^0_{N'} & \mathbf{MI}^2_{N'} & \mathbf{MI}^3_{N'} & \ldots & \mathbf{MI}^s_{N'} \end{bmatrix}. \tag{18}$$

Let $\mathcal{C}$ represents covariance matrix of $\mathbb{MI}$ defined as

$$\mathcal{C} = \frac{1}{N'}\mathbb{MI}_c^T\mathbb{MI}_c, \tag{19}$$

where $\mathbb{MI}_c$ is centred matrix obtained by subtracting mean of each column, $\boldsymbol{\mu}$, of $\mathbb{MI}$, i.e., $\mathbb{MI}_c = \mathbb{MI} - \boldsymbol{\mu}$. Now, to identify the orthogonal active directions of moment space, the eigenvectors are computed via their eigenvalue decomposition, which can be written as

$$\mathcal{C} = \mathbf{W}\boldsymbol{\Lambda}\mathbf{W}^T. \tag{20}$$

Herein, $\mathbf{W} = \{\mathbf{w}_1, \mathbf{w}_2, \ldots, \mathbf{w}_s\}$ is an $[s \times s]$ matrix whose columns are orthogonal eigenvectors ($\mathbf{w}_k \in \mathbb{R}^{1\times s}$), which spans the new basis to form an eigenspace. Moreover, $\boldsymbol{\Lambda} = \text{diag}(\lambda_1, \lambda_2, \ldots, \lambda_s)$, with λ_i's being the eigenvalues sorted in descending order $\lambda_1 \geq \lambda_2 \geq \cdots \geq \lambda_s$, which represents the variance resolved along the corresponding eigenvectors. Based on the above decomposition and the variance-based SA, one can use Lamboni et al.'s [60] generalised sensitivity indices for multivariate outputs using the eigenmodes or principal components ($\mathbb{DI}$) obtained with first K eigenvectors which covers at least 95% of the empirical variance, i.e., $\mathbb{DI} = (\mathbb{MI} + \boldsymbol{\mu})\{\mathbf{W}\}_{k=0}^K$. The generalised first-order sensitivity index for the ith variable is defined as

$$GSI_i = \sum_{k=1}^{K} \frac{\lambda_k}{V(Y)} SI_{i,k}, \tag{21}$$

and the generalised total-order sensitivity index for the ith variable is evaluated as

$$GSI_{T_i} = \sum_{\omega_i} GSI_{\omega_i}, \tag{22}$$

where ω_i includes all the components in the ANOVA decomposition with all subscripts including i. $SI_{i,k}$ in Eq. (21) are the first-order sensitivity indices of the ith variable, evaluated as in Eq. (16a), on the new orthogonal basis $w_{i,k}$. Under this new setting it can be written as

$$SI_{i,k} = \frac{V_{i,k}}{V_k}, \tag{23}$$

where $V_{i,k}$ is the partial variance of the kth eigenmode caused by the variation in the ith parameter and V_k is equal to the eigenvalue λ_k. The generalised sensitivity indices in Eq. (22) give the significance of the parameters for $\mathcal{MI}^s$ in the same way as the sensitivity indices do in the univariate output case in Eq. (17). For more details, interested readers should refer to [59,60].

3.4.2. Covariance decomposition approach

Gamboa et al. [31] proposed the covariance decomposition approached, which is based on the Hoeffding–Sobol decomposition as in Eq. (12). It can be generalised for any arbitrary number of output variables,

$$\begin{aligned}\mathbf{MI} = \mathbf{MI}^r_0 + \sum_{i=1}^{n} \mathbf{MI}^r_i(t_i) + \sum_{i=1}^{n}\sum_{j=i+1}^{n} \mathbf{MI}^r_{ij}(t_i, t_j) + \cdots \\ + \mathbf{MI}^r_{1,\ldots,n}(t_1, \ldots, t_n), \quad r = 1, 2, \ldots, s,\end{aligned} \tag{24}$$

which implies that the covariance matrix of the model output can be partitioned into a sum of covariance matrices as follows:

$$\begin{aligned}\mathcal{C}\left(\mathcal{MI}^s\right) = \mathcal{C}\left(\mathbf{MI}^0, \ldots, \mathbf{MI}^s\right) = \sum_{i=1}^{n} \mathcal{C}_i\left(\mathbf{MI}^0, \ldots, \mathbf{MI}^s\right) \\ + \sum_{i=1}^{n}\sum_{j=i+1}^{n} \mathcal{C}_{i,j}\left(\mathbf{MI}^0, \ldots, \mathbf{MI}^s\right) + \cdots \\ + \mathcal{C}_{1,2,\ldots,n}\left(\mathbf{MI}^0, \ldots, \mathbf{MI}^s\right).\end{aligned} \tag{25}$$

The above equation is equivalent to the decomposition of variance in Eq. (13) which is used for the scalar output. This implies that the main effect indices can be obtained as $SI_i = V_i/V(M^{0,0,0}) = \mathcal{C}_i/\mathbf{C}(M^{0,0,0})$. Gamboa et al. used this idea to project $\mathcal{C}$ onto a scalar through multiplication by an identity matrix and then taking its trace (Tr) as

$$\begin{aligned}\mathrm{Tr}\left[\mathcal{C}\left(\mathcal{MI}^s\right)\right] &= \mathrm{Tr}\left[\mathcal{C}\left(\mathbf{MI}^0,\ldots,\mathbf{MI}^s\right)\right]\\ &= \sum_{i=1}^{n}\mathrm{Tr}\left[\mathcal{C}_i\left(\mathbf{MI}^0,\ldots,\mathbf{MI}^s\right)\right]\\ &\quad+\sum_{i=1}^{n}\sum_{j=i+1}^{n}\mathrm{Tr}\left[\mathcal{C}_{i,j}\left(\mathbf{MI}^0,\ldots,\mathbf{MI}^s\right)\right]+\\ &\quad\cdots+\mathrm{Tr}\left[\mathcal{C}_{1,2,\ldots,n}\left(\mathbf{MI}^0,\ldots,\mathbf{MI}^s\right)\right].\end{aligned} \tag{26}$$

On the basis of the above, the multivariate main effect indices of the ith variable can be obtained as

$$GSI_i\left(\mathcal{MI}^s\right) = \frac{\mathrm{Tr}\left[\mathcal{C}_i\right]}{\mathrm{Tr}\left[\mathcal{C}\right]}, \tag{27}$$

while the multivariate total effect sensitivity indices are given as

$$GSI_{T_i}\left(\mathcal{MI}^s\right) = \frac{\mathrm{Tr}\left[\mathcal{C}_i\right]+\sum_{i=1}^{n}\sum_{j=i+1}^{n}\mathrm{Tr}\left[\mathcal{C}_{ij}\right]+\cdots+\mathrm{Tr}\left[\mathcal{C}_{1,2,\ldots,n}\right]}{\mathrm{Tr}\left[\mathcal{C}\right]}. \tag{28}$$

As the trace, $\mathrm{Tr}\left[\mathcal{C}\left(\mathcal{MI}^s\right)\right]$ is equal to the sum of variances of all elements of $\mathcal{MI}^s$ in Eq. (26), GSI_i can be interpreted as the expected percentage reduction in the total variance of the outputs, which is obtained when variable t_i is kept fixed. Garcia-Cabrejo and Valocchi [61] also demonstrated that if the covariance of $\mathcal{MI}^s$ is fully captured by the first K eigenvectors, then GSI_i obtained from this method are equal to GSI_i from *output decomposition approach* in the previous subsection. We will base our SA using the covariance decomposition approach in the present case. Unlike in time series data, the dimensionality of moment space is not extensively high in our case. Furthermore, the covariance decomposition approach reduces the possibility of approximation error during the dimension reduction and numerical inaccuracies resulting from using the output decomposition method during eigendecomposition.

3.5. Selection of sensitive parameters

After obtaining the sensitivity indices, a subset of the highly sensitive parameters, whose variation influence significantly the QoI while ignoring those that do not contribute significantly towards design improvement against QoI. Therefore, only a small subset of sensitive parameters are allowed to vary during shape optimisation, and others are kept fixed, thereby accelerating the shape optimisation process. The selection of a subset of sensitive parameters can be made either based on the available computational budget [10,13], using a predefined threshold value (such as ϵ) [62,63] or clustering the parameters into groups of high and low sensitive ones based on their sensitivity indices [16,26]. In the first approach, for instance, if only a limited number of design evaluations are allowed to be performed during optimisation, then the designer will favour selecting a smaller subset of only highly sensitive parameters to achieve maximum possible design improvement within the available computational budget. A threshold ϵ is defined based on a statistically significant value in the second approach. Any parameter with sensitivity indices greater or equal to ϵ is included in the analysis, and others are kept fixed. The second approach is more favourable and widely practised among these three approaches. It provides the subset of sensitive parameters that are statistically sufficient to redefine the problem with a smaller set of parameters. However, the setting of ϵ is important as the smaller value may result in selecting more parameters, and a larger value may form the subset containing fewer sensitive parameters. For complex analyses, $\epsilon = 0.05$ is widely used [62]. The influence of ϵ on the selection of significantly sensitive parameters will be analysed in Section 5.

4. Test cases

To experimentally demonstrate geometric moments' capability to make an informed decision regarding the parametric sensitivity, we use the wave resistance coefficient, C_w, as a physical criterion. C_w is part of the overall resistance affecting the movement of objects on or near the free surface of oceans, lakes and rivers. It reflects the energy spend for creating the free-surface waves following the moving body. Although the overall resistance of the ship is composed of different components, C_w is a vital component and especially prominent for relatively full hull forms travelling at high speeds. It is noteworthy that C_w is highly sensitive to local features of the hull so that a significant reduction can be achieved without affecting the overall cargo capacity. Similar to geometric moments, C_w is affected by the distribution of the hull's shape, and it can be used as a physics-informed shape signature. Minimising this resistance at the preliminary design stage is crucial, but its evaluation can be computationally demanding.

4.1. Relation of moments with wave resistance coefficient

Our motivation to investigate the utility of moments in SA for ship design stems from the extensive use of *SAC (Sectional Area Curve)* in Computer-Aided Ship Design and Hydrodynamic Analysis. SAC is a function $S(x)$ of 2D zeroth-order moments describing the longitudinal variation of the area of ship sections below the waterline. In [64], it is stated: *"A SAC provides an effective and simple description of global geometric properties. At the same time, it is closely related to the resistance and propulsion performance of a ship. From this point of view, the ship hull form distortion approach based on SAC transformation is one of the most effective global design methods for the preliminary design stage"*. In analogous spirit, [65] stresses that *"geometric properties of SAC have a decisive effect on the global hydrodynamic properties of ships"*. Historically, the importance of SAC in ship design has been initiated back in the 1950s with the introduction of Lackenby transformation [66] for modifying SAC, which has been further enriched in the context of modern CAD representations and used in ship-design optimisation, see, e.g., in [67,68].

Furthermore, linear wave-resistance analysis performed by eminent hydrodynamicists, e.g., E.O. Tuck [69,70], J.V. Wehausen [71], has revealed the importance of the longitudinal rate of change of cross-sectional area, i.e., $S'(x)$, which determines the strength of the Kelvin-source distribution used to model the disturbance caused by the body as it moves on the sea's free-surface. It is worth noticing that the flow around a slender ship moving on the free surface with a constant velocity can be represented by using an appropriate source–sink distribution along its centre plane. The strength of these sources is proportional to the longitudinal rate of change of the ship's cross-sectional area [69,71], and this aspect can be well captured by geometric moments, especially those of higher order. In fact, an early derivation for the evaluation of C_w for slender ships, known as Vosser's integral, reveals explicit dependence on the longitudinal derivative of the cross-sectional area [71], i.e., $S'(x) = \frac{\mathrm{d}}{\mathrm{d}x}S(x)$ where $S(x) = \int_{\Omega(x)}\mathrm{d}y\mathrm{d}z$ is the cross-sectional area, and $\Omega(x)$ denotes the cross-section of a

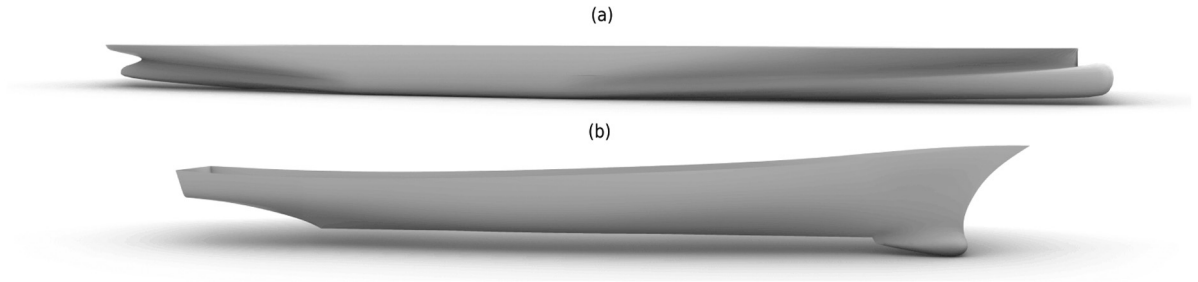

Fig. 2. Three dimensional CAD geometries of (a) PD and (b) DTMB 5415 hull models used as test cases for the proposed approach.

Fig. 3. Three dimensional design variations of the PD hull (on the left) and DTMB 5415 hull (on the right) generated with 26 and 27 design parameters defined using PD- and GMF-based parameterisation, respectively. These design variations can also be visualised in a video at https://bit.ly/3BiB9wZ. For PD hull, parameterisation is performed on the submerged part below the waterline, and for both hull their geometric moments are evaluated for the submerged part.

ship hull at the longitudinal position x. Let now $m_p = \int_o^L x^p S'(x)\mathrm{d}x$ be the p-th order moment of $S'(x)$ with $x = 0$ and $x = L$ corresponding to the stern and bow tips of the hull, respectively. Assuming that $S(0) = S(L) = 0$ we get:

$$m^p = -p \int_0^L x^{p-1} S(x)\mathrm{d}x = -p \int_0^L \int_{\Omega(x)} x^{p-1}\mathrm{d}x\mathrm{d}y\mathrm{d}z, \tag{29}$$

which leads to

$$m^p = -pM^{p-1,0,0}, \tag{30}$$

where $M^{p-1,0,0}$ is a component of the hull's geometric moments vector of order $s = p + q + r = p - 1$ (see Eq. (2)). Thus, p-order 1D moments of $S'(x)$ are directly linked to $(p-1)$-order 3D longitudinal moments of the hull. These physics-informed moments are included in the set of moments used for building the SSV we use for SA.

4.2. Parametric modellers

To validate our claim regarding geometric moments, we used two different test cases based on a different type of parameterisation, namely Procedural Deformation (PD) [27,72] and Global Modification Function (GMF) [4]. PD is used for the parameterisation of the hull shown in Fig. 2(a), which shares some closeness to the well known KCS[1] ship hull model, and shall be referred to as the *PD hull* from this point forward in this paper. GMF is used to parametrise a DTMB 5415[2] naval ship model (see Fig. 2(b)), an early and open to the public version of the USS Arleigh Burke destroyer DDG 51, which is another extensively used benchmark ship model for shape optimisation problems.

PD creates a high-level parameterisation via coupling free-form features with control points of the underlying surface representation through linear procedural relations. This results in a fully feature-driven parameterisation, i.e., each parameter defines and alters a specific feature of the PD hull, such as the length, width or length of the bulbous bow. This parameterisation provides both local and global shape modification. GMF is a grid modification approach performed using a shape modification function based on vector-valued functions defined on a design grid. These functions are defined with the objective that during modification, the underlying structure of the design should be preserved, the design grid used for simulation to evaluate C_w does not have to regenerate, and a prescribed degree of similarity should be maintained. However, unlike PD, the parameterisation obtained from GMF is not feature-driven as varying a parameter may alter a specific feature and features in its neighbourhood. Variations of hull designs obtained from both types of parameterisation are shown in Fig. 3.

4.2.1. Procedural deformation (PD)

Let $\mathcal{G}$ be a member of a rich class of objects in an ambient space $\mathcal{A} \subseteq \mathbb{R}^3$. The PD-based parametric modeller, $\mathcal{P}$, used in this work is based on the technique proposed by Kostas et al. [27], which for any $\mathbf{t} \in \mathcal{X}$ produces a new shape $\mathcal{G}' = \mathcal{P}(\mathbf{t})$. In this case, $\mathcal{P}(\mathbf{t})$ is a vector function $\mathbb{R}^n \to \mathcal{A}$ that defines the underlying geometry of $\mathcal{G}$, which corresponds to $\mathbf{t} = t_i, i = 1, 2, \ldots, 26$. As the PD in this case adopts the NURBS (Non-Uniform Rational B-splines) surface representation, $\mathcal{P}(\mathbf{t}) = N(CG(\mathbf{t}); \Omega)$, where $N : \mathbb{R}^2 \to \mathbb{R}^3$ is a vector-valued function that maps each point of the two dimensional domain, Ω, to a point on the surface bounding $\mathcal{G}$. Here, $CG(\mathbf{t})$ represents the *control cage* of $\mathcal{G}$, which maps $\mathbf{t}$ onto the control points of CG. Parameters in $\mathbf{t}$ are classified in four categories, namely global, local, semi-global and shape transition parameters, providing shape modification of different nature. The parametric definition on the hull geometry is shown in Fig. 4.

The global parameters, hull length at waterline, beam and depth, are the most shape influential. Typically, these parameters are predefined during the design process based on the customer requirements; therefore, these are kept fixed in our analysis. The local parameters, such as parameters defining lengths at flat side

[1] http://www.simman2008.dk/KCS/container.html.
[2] http://www.simman2008.dk/5415/combatant.html.

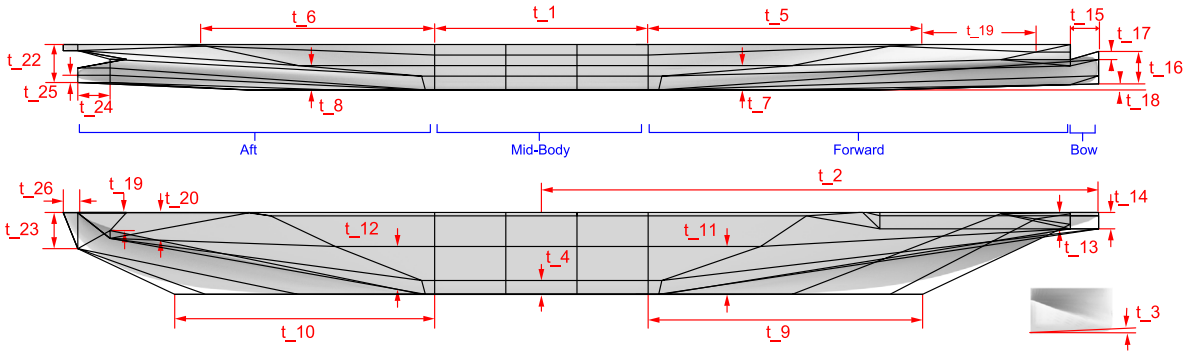

Fig. 4. Parameterisation of PD hull adopted by the PD-based parametric modeller.

and bottom at the aft and forward (t_5, t_6, t_9, t_{10}), bulb bow (t_{14} - t_{17}), stern (t_{22} - t_{24}), bilge radius (t_4), shaft (t_{25}, t_{26}) dimensions, etc., affect small areas of the geometry but can cause significant changes on C_w [27]. Semi-global parameters affect relatively large hull areas, such as the length and position of the mid-ship body (t_1 and t_2). Transition parameters are also local, controlling the transition between different sections of the shape, for instance, the transition from mid-ship to bow (t_{19}). In this case, all these parameters are defined as

$$t_i = \hat{t}_i \cdot f_i\,(t_1, t_2, \ldots t_{26})\,, \quad \hat{\mathbf{t}} \in [0,\,1],\ i = 1, 2, \ldots, 26, \tag{31}$$

where $\hat{t}_i$ is the ith non-dimensional version of t_i bounded by [0,1] and f_i are affine functions of these parameters defining the procedural relation and is specified internally by the developer. During shape modification, [27] recommends using $\hat{\mathbf{t}}$ for supporting robustness by avoiding setting parametric values that would result in creating invalid and implausible geometries. Once the values of global parameters and $\hat{\mathbf{t}}$ are given, the control cage, shown in Fig. 4, is automatically constructed. For further details on the formulation of this parameterisation, interested readers should refer to [27].

4.2.2. Global modification function (GMF)

Let be given a set of coordinates $\boldsymbol{\zeta} \in \mathcal{G} \subset \mathbb{R}^{\overline{n}}$, with $\overline{n} = 1, 2, 3$, and assume that the design variables set $\mathbf{t}$ defines a continuous shape modification vector $\boldsymbol{\delta}(\boldsymbol{\zeta}, \mathbf{t}) \in \mathbb{R}^{\hat{n}}$, with $\hat{n} = 1, 2, 3$, which for any $\mathbf{t} \in \mathcal{X}$ modifies each $\boldsymbol{\zeta} \in \mathcal{G}$ of the baseline shape to a new shape $\boldsymbol{\zeta}' \in \mathcal{G}'$ as

$$\boldsymbol{\zeta}' = \boldsymbol{\zeta} + \boldsymbol{\delta}(\boldsymbol{\zeta}, \mathbf{t}), \tag{32}$$

where $\mathcal{G}'$ is the modified version of the $\mathcal{G}$. In the present work, $\boldsymbol{\delta}(\boldsymbol{\zeta}, \mathbf{t})$ is defined using a recursive combination of $n = 27$ shape modification vectors over a hyper-rectangle embedding the demi hull:

$$\boldsymbol{\psi}_i(\boldsymbol{\zeta})\ :\ \mathcal{A} = [0, L_{\zeta_1}] \times [0, L_{\zeta_2}] \times [0, L_{\zeta_3}] \in \mathbb{R}^3 \longrightarrow \mathbb{R}^3, \tag{33}$$

with $i = 1, \ldots, n$. Specifically,

$$\boldsymbol{\delta}(\boldsymbol{\zeta}, \mathbf{t}) = \boldsymbol{\delta}_n, \tag{34}$$

where

$$\boldsymbol{\delta}_i(\boldsymbol{\zeta}, \mathbf{t}) = t_i \boldsymbol{\psi}_i(\boldsymbol{\zeta}), \quad \text{with} \quad \begin{cases} \boldsymbol{\zeta} = \boldsymbol{\zeta} + \boldsymbol{\delta}_{i-1} \\ \boldsymbol{\delta}_1 = 0 \end{cases} \tag{35}$$

The coefficients $\{t_i, i = 1, \ldots, n \in \mathbb{R}\}$ are the design parameters and forms a 27-dimensional initial (original) design space $\mathcal{X}$. For modification the shape functions are defined as

$$\boldsymbol{\psi}_i(\boldsymbol{\zeta}) := \prod_{j=1}^{3} \sin\left(\frac{a_{ij}\pi\,\zeta_j}{L_{\zeta_j}} + r_{ij}\right) \mathbf{e}_{q(i)}. \tag{36}$$

In Eq. (36), $\{a_{ij}, j = 1, 2, 3\} \in \mathbb{R}$ define the degree of the function along jth axis, $\{r_{ij}, j = 1, 2, 3\} \in \mathbb{R}$ are the corresponding spatial phases and $\{L_{\zeta_j}, j = 1, 2, 3\} \in \mathbb{R}$ are the hyper-rectangle edge lengths; $\mathbf{e}_{q(i)}$ is a unit vector. Modifications are applied along ζ_1, ζ_2, or ζ_3, with $q(i) = 1, 2,$ or 3 respectively. Details of setting parameters can be found in [4].

The objective of using two different types of parameterisation on two different hulls is to see if geometric moment invariants capture the sensitivity of parameters under various design settings.

4.3. Hydrodynamic solver and setup

Two inviscid solvers are for two ship hulls, both symmetric with respect to the xz-plane. For the one hull referred to as the PD hull model, the PD parameterisation is used, while for the other hull, referred to in the literature as the DTMB hull, we employ the GMF parameterisation.

PD hull model: Hydrodynamic calculations to estimate C_w for the PD hull are performed using the Isogeometric Analysis-based Boundary Element Method (IGA-BEM) developed by Belibassakis et al. [7]. This solver applies the Isogeometric Analysis (IGA) [73] for solving the boundary integral equation (BIE) associated with the linearised Neumann–Kelvin formulation for the calculation of C_w of ships. The IGA concept is based on exploiting the same NURBS basis used to represent the exact geometry of the hull for approximating the singularity distribution of the associated BIE, or, in general, the dependent physical quantities. In BIE, the dependent/unknown variable is the density of Neumann–Kelvin sources distributed over the hull's wetted surface, which is accurately represented with parametric NURBS surfaces or a collection of smoothly joined NURBS patches; referred to as multi-patch NURBS surface. In our case, the PD hull is composed of a signal cubic NURBS surface with 108 control points, whose iso-mesh is shown in Fig. 5 and simulation is performed on the unit scaled right demi-hull.

DTMB hull model: Hydrodynamic simulations of this hull model are conducted using the code WARP (Wave Resistance Program), developed at CNR-INM. C_w computations are based on linear potential flow theory using Dawson (double-model) linearisation. The frictional resistance is estimated using a flat-plate approximation based on the local Reynolds number. Details of equations, numerical implementations, and validation of the numerical solver are given in [28]. As with the DTMB hull model, simulations are performed for the demi-hull. Fig. 5(b) shows the computational grid used for the simulation. The computational domain for the free-surface is defined within $1L_{\text{pp}}$ upstream, $3L_{\text{pp}}$ downstream, and $1.5L_{\text{pp}}$ sideways. A total of 75 × 20 grid nodes are used for the free surface, whereas 90 × 25 nodes are used for

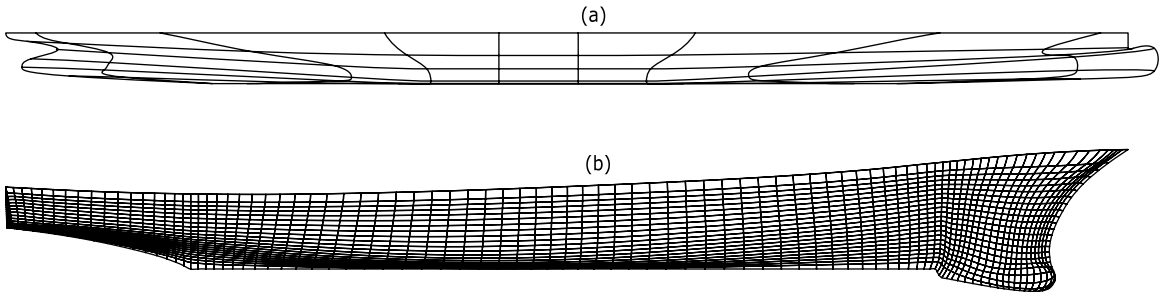

Fig. 5. Computational grid of (a) PD hull and (b) DTMB 51 415 hull used during the simulation for approximation of C_w.

Table 1
Main particular, test conditions and C_w values of PD hull and DTMB 5415 hull.

Quantity	Symbol	Unit	Value	
			DTMB hull	PD Hull
Volume of displacement	∇	m^3	8419.31	5112.56
Wetted surface area	S	m^2	2974.23	2076.56
Length at waterline	Lwl	m	142.73	100.00
Max beam at waterline	Bwl	m	19.06	16.25
Draft	T	m	6.15	4.51
Water density	ρ	kg/m^3	998.50	
Kinematic viscosity	ν	m^2/s	1.09E−6	
Gravity acceleration	g	m/s^2	9.80	
Froude number	Fr	–	0.25	
Wave resistance coefficient	C_w	–	1.0531E−03	1.0678E−04

the hull discretisation. The main particulars, test conditions and C_w values for both type hulls are given in Table 1.

5. Results and discussion

This section demonstrates the effectiveness of geometric moment invariants for evaluating parametric sensitivities using various experiments on the previously described test cases. We first provide the results of geometric moment invariants for PD and DTMB hull models and then discuss the Sensitivity Analysis (SA) results with respect to Shape-Signature Vector (SSV) and C_w for both hull types, along with the correlation between the results. Finally, for both test cases, we present the optimisation results performed in the sensitivity spaces evaluated with SSV and C_w.

5.1. Moment evaluation

As mentioned before, for any shape satisfying the conditions mentioned in Section 3.2, there exist geometric moments of arbitrary order. In this work, we mainly focus on performing SA with respect to fourth-order geometric moments invariant to the translation and scaling. This choice results from two facts:

1. Higher-order moments can be sensitive to noise acquisition [25]. The risk of numerical inaccuracies, specifically due to the use of finite-precision arithmetics, also increases as we move towards evaluating high-order moments [23]. Therefore, it could be challenging to include moments of order greater than 10 as computational complexity increases with the order.
2. Literature review in various application areas, e.g., kinetic equations [74] and shape retrieval [56], reveals that it is unlikely to use moments of order higher than 4.

Thus, SSV of order $s = 4$ ($\mathcal{MI}^4$) is used to evaluate the sensitivity of parameters of both test cases. In $\mathcal{MI}^4$, there are 1, 6, 10 and 15 components of 0*th*- 2*nd*-, 3*rd*- and 4*th*-order geometric moments, respectively. The values of these invariants for two hulls are shown in Table 2. As explained earlier in Section 3, all the moment invariants of first-order are zero, while the zeroth-order moment is equal to one due to its scale invariance. Therefore, the effect of sensitivity of parameters in the case of zeroth-order is measured with $M^{0,0,0}$ instead of $MI^{0,0,0}$, as $M^{0,0,0}$ defines the volume of the shape.

5.2. Sensitivity analysis of PD hull model

As described earlier, the PD hull is parameterised with 26 procedural parameters, so a 26-dimensional design space is created while keeping the baseline hull at the centroid of the design space. To commence the SA, the design space is sampled with $N' = 9000$ samples using a progressive sampling technique [10, 75]. This sampling technique is based on the space-filling criterion, searching the design space in the class of Latin-Hypercube to ensure a uniformly distributed and diverse set of samples. $\mathcal{MI}^4$ and C_w of designs are evaluated on the basis of the setting described in Sections 3.2 and 4.3, respectively. Afterwards, two different datasets are created, the first containing the design parameter values as independent variables and C_w as dependent variables. The second dataset is composed of $\mathcal{MI}^4$ as dependent variables. Afterwards, Sobol's global SA for univariate output is performed to measure the sensitivity of parameters towards C_w, and multivariate output Sobol's analysis with covariance decomposition approach is utilised to estimate the parameters' sensitivity to $\mathcal{MI}^4$. In the remainder of this section, we first discuss the results on the sensitivity of parameters with respect to C_w (shown in Fig. 6) and then we present the results of parameters' sensitivity measured with respect to the zeroth- to the fifth-order (shown in Figs. 7 and 8) SSV to observe how the sensitivity of parameters varies with the increment in the order. Finally, we compare the sensitivity indices of parameters evaluated with $\mathcal{MI}^4$ and C_w.

To select the set of sensitive parameters, a threshold is set equal to $\epsilon = 0.05$ [62]. From Fig. 6, it can be seen that in case of C_w, 4 out of 26 parameters, t_1, t_2, t_6 and t_{19}, have a sensitivity index greater than ϵ and thus regarded as the C_w sensitive parameters. Among these parameters, t_1 and t_2 have a substantially higher sensitivity index, defining the mid-body length and position. These parameters are of semi-global nature and have the highest impact on the hull's shape after the three global parameters, and thus, they significantly affect the variation of C_w. The next two sensitive parameters, t_6 and t_{19}, have a sensitivity index close to ϵ. Here, t_6 is a local parameter, which modifies the flat-of-side length at the aft of the hull and t_{19} is the transition parameter defining the interaction of the bow and bulb of the hull. These results align with the literature [10] as parameters associated around the bulbous bow segment of the hull are known to have a significant influence on C_w.

Table 2
Geometric moment invariants up to 4th-order evaluated for the PD and DTMB hull models.

Designs	$M^{0,0,0}$	$MI^{2,0,0}$	$MI^{0,2,0}$	$MI^{0,0,2}$	$MI^{1,1,0}$	$MI^{1,0,1}$	$MI^{0,1,1}$	$MI^{0,0,3}$
DTMB hull	8.4193E+03	2.3151	4.1970E−02	6.9840E−03	0	−2.3789E−02	0	−3.3039E−04
PD hull	5.1126E+03	1.7426	5.7126E−02	5.4962E−03	0	−3.8124E−03	0	−4.7635E−05
	$MI^{0,1,2}$	$MI^{0,2,1}$	$MI^{0,3,0}$	$MI^{1,0,2}$	$MI^{1,1,1}$	$MI^{1,2,0}$	$MI^{2,0,1}$	$MI^{2,1,0}$
DTMB hull	0	1.0767E−03	0	2.7862E−03	0	−9.0788E−03	2.4529E−03	0
PD hull	0	3.7467E−04	0	−6.2258E−05	0	−4.8513E−03	1.7167E−02	0
Designs	$MI^{3,0,0}$	$MI^{0,0,4}$	$MI^{0,1,3}$	$MI^{0,2,2}$	$MI^{0,3,1}$	$MI^{0,4,0}$	$MI^{1,0,3}$	$MI^{1,1,2}$
DTMB hull	4.4042E−01	1.3333E−04	0	2.2588E−04	0	3.9970E−03	−8.8414E−04	0
PD hull	1.5272E−01	5.5021E−05	0	3.1210E−04	0	6.7697E−03	−2.8814E−05	0
Designs	$MI^{1,2,1}$	$MI^{1,3,0}$	$MI^{2,0,2}$	$MI^{2,1,1}$	$MI^{2,2,0}$	$MI^{3,0,1}$	$MI^{3,1,0}$	$MI^{4,0,0}$
DTMB hull	−5.5388E−04	0	2.2982E−02	0	6.0453E−02	−2.2388E−01	0	12.3709
PD hull	−1.8780E−04	0	9.2384E−03	0	6.3636E−02	−2.3872E−02	0	6.5083

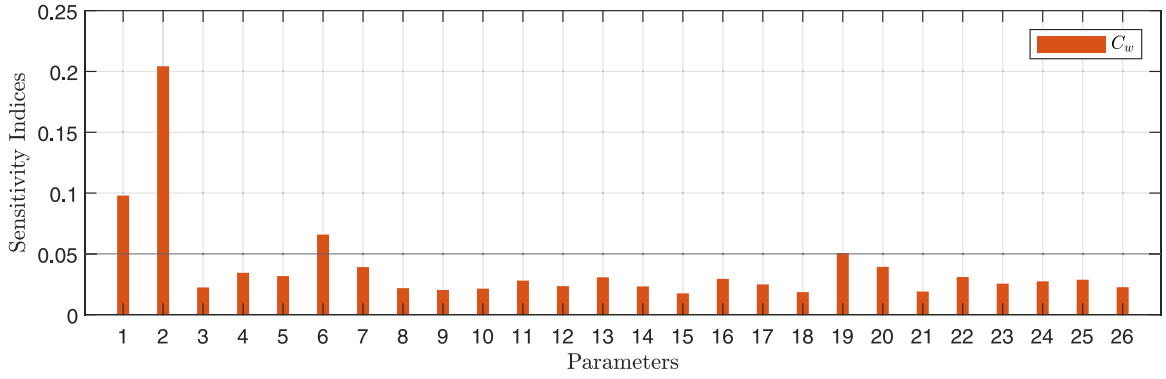

Fig. 6. Sensitivity indices of PD hull's 26 design parameters obtained using Eq. (17) with respect to C_w.

The parametric sensitivity indices obtained with SSV are shown in Fig. 7. We will start the discussion with the results related to $\mathcal{MI}^0$, which only consists of the zeroth-order moment, $\mathbf{M}^0$, i.e., the volume of the submerged part of the hull. In this case, there are three parameters, t_1, t_4 and t_6, sensitive to $\mathcal{MI}^0$. The reader should recall that, among these parameters, t_1 and t_6 are sensitive to C_w, which means that $\mathcal{MI}^0$ is able to capture 50% of the parametric sensitivity to C_w. Obviously, the parameter t_1 is more sensitive to volume as it modifies the length of the mid-body of the hull. However, as the volume does not get affected by changing the position of the mid-ship, t_2, which is a third sensitive parameter with regards to C_w, has a negligible effect on $\mathcal{MI}^0$. Interestingly, in the case of $\mathcal{MI}^2$, similar with respect to C_w, there are four parameters, t_1, t_2, t_5 and t_6, with indices higher than 0.05 and out of these four sensitive parameters, three parameters, t_1, t_2 and t_6, are also sensitive to C_w. Note that the sensitivity index of t_2 is now close to that obtained with C_w, which means that $\mathcal{MI}^2$ can capture the sensitivity of the shape caused by varying mid-body position (i.e., the parameter t_2). More importantly, the parameters, t_1, t_2 and t_6 are the top three most sensitive parameters both with respect to C_w and $\mathcal{MI}^2$. The parameter, t_5, which is only sensitive to $\mathcal{MI}^2$, is local by definition and modifies the flat-of-side at the forward part of the hull.

From the results depicted in Fig. 7, it can be seen that via $\mathcal{MI}^2$ we are able to capture the sensitivity of not only the semi-global parameters (t_1, t_2) but also the sensitivity of the local parameters (t_5, t_6), which means that in comparison with $\mathcal{MI}^0$, $\mathcal{MI}^2$ is more capable of reflecting the sensitivity of parameters with respect to C_w. For the transition parameter, t_{19}, its sensitivity index has increased, but it is still far from being categorised as sensitive. Therefore, geometric moment invariants of higher order may be required.

In the case of $\mathcal{MI}^3$ and $\mathcal{MI}^4$, the sensitive parameters remain the same as in the case of $\mathcal{MI}^2$. However, the sensitivity indices of almost the entire set of parameters differ from what was obtained with $\mathcal{MI}^0$ and $\mathcal{MI}^2$. As we moved from $\mathcal{MI}^0$ to $\mathcal{MI}^4$, the domination of sensitivity indices of highly sensitive parameters (t_1, t_2) reduces and sensitivity indices of other parameters increases. Primarily, this is prominent for t_1, whose sensitivity indices decreases significantly from 0.7625 ($\mathcal{MI}^0$) to 0.2889 ($\mathcal{MI}^4$). However, from $\mathcal{MI}^3$ to $\mathcal{MI}^4$ sensitivity indices remain similar. Another essential point to note here is that, when sensitivity analyses are performed with $\mathcal{MI}^4$, the sensitivity index of transition parameter t_{19}, which is sensitive with respect to C_w and is the only parameter that could not be categorised as sensitive to geometric moments, increases monotonically as 0.0045 ($\mathcal{MI}^0$), 0.0122 ($\mathcal{MI}^2$), 0.0212 ($\mathcal{MI}^3$) and 0.0447 ($\mathcal{MI}^4$). It can be seen that at $\mathcal{MI}^4$, the sensitivity index of t_{19} becomes very close to one obtained with C_w. This indicates that as we move towards higher-order geometric moments, we capture more detailed geometric information of the hull, including its local features. To further validate this, we increased the order of SSV from 4 to 5 and analysed the behaviour of parametric sensitivities with the inclusion of 5th order moments in SSV (i.e., $\mathcal{MI}^5$). It can be seen from Fig. 8 that parameters sensitive with respect to $\mathcal{MI}^4$ are also sensitive to $\mathcal{MI}^5$. However, the sensitivity indices obtained with $\mathcal{MI}^5$ tends to be similar to ones obtained with C_w. Summary of these sensitivity results is provided in Table 3.

Note the correlation results discussed above are evaluated at $\epsilon = 0.05$. As stated in Section 3.5, when the value of ϵ changes the then parameters sensitive to both C_w and $\mathcal{MI}^s$ change. For

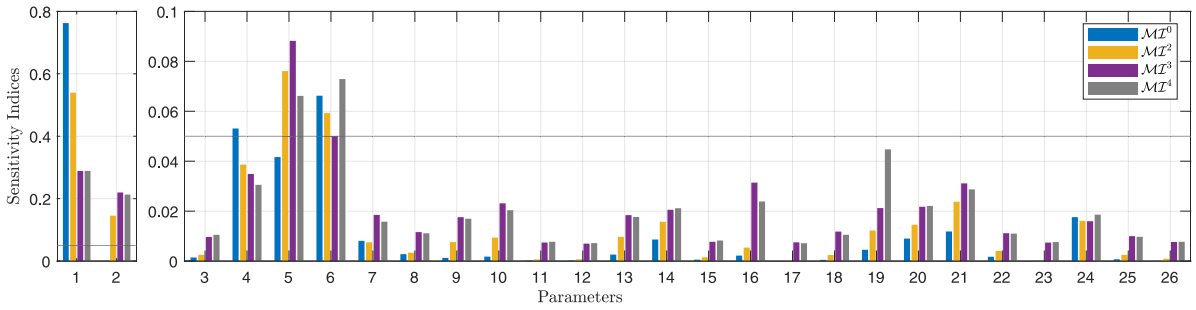

Fig. 7. Sensitivity indices of PD hull's 26 design parameters obtained using Eq. (28) with respect to $\mathcal{MI}^0$, $\mathcal{MI}^2$, $\mathcal{MI}^3$ and $\mathcal{MI}^4$.

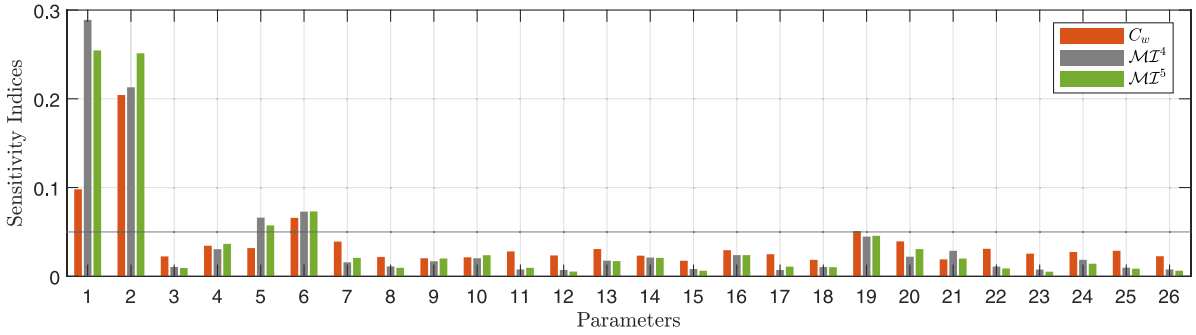

Fig. 8. Sensitivity indices of PD hull's 26 design parameters obtained with respect to 4th and 5th order SSV (i.e., $\mathcal{MI}^4$ and $\mathcal{MI}^5$) and wave resistant coefficient (C_w).

Table 3
Sensitive parameters of PD hull with respect to C_w and $\mathcal{MI}^s$ with $s = 0/2/3/4/5$.

QoI	Sensitive parameters	NMSE	Similarity
C_w	t_1, t_2, t_6, t_{19}	–	–
$\mathcal{MI}^0$	t_1, t_4, t_6	0.7399	58%
$\mathcal{MI}^2$	t_1, t_2, t_5, t_6	0.4822	75%
$\mathcal{MI}^3$	t_1, t_2, t_5, t_6	0.2221	75%
$\mathcal{MI}^4$	t_1, t_2, t_5, t_6	0.2146	75%
$\mathcal{MI}^5$	t_1, t_2, t_5, t_6	0.1856	75%

instance, in Fig. 6, when we set $\epsilon = 0.1$, we will have only one parameter in the subset of significantly sensitive parameters and setting $\epsilon = 0.075/0.05/0.04/0.03$ will result in 2/4/4/10 sensitive parameters, respectively, in the final subset. Similarly, in Fig. 7, when ϵ is equal to 0.04 and 0.05 then parameters sensitive to $\mathcal{MI}^0$ are $[t_1, t_4, t_5, t_6]$ and $[t_1, t_4, t_6]$, respectively. In both cases, $[t_1, t_4]$ are also sensitive to C_w. So, respectively of the specific value adopted for ϵ, one can make a good preliminary estimation of sensitive parameters at a significantly reduced computational cost. A commonly used threshold value is $\epsilon = 0.05$ [62,63], specifically for selecting a subset of significantly sensitive parameters to construct a design space of reduced dimension. This is the value used in this work.

Moreover, as the parametric sensitivities are evaluated based on SSD [10], we also perform an experiment where the number of samples is varied against the sensitivity indices of parameters. Fig. 9 show the sensitivity indices of the top 5 sensitive parameters (t_1, t_2, t_4, t_5 and t_6) evaluated with respect to $\mathcal{MI}^4$ versus the number of samples. It can be seen that sensitivity indices vary as the sample size increases, especially for parameter t_1, which is the topmost sensitive parameter. However, sensitivity indices reach a plateau after a sample size equal to 1000, sufficient to reach true parametric sensitivities.

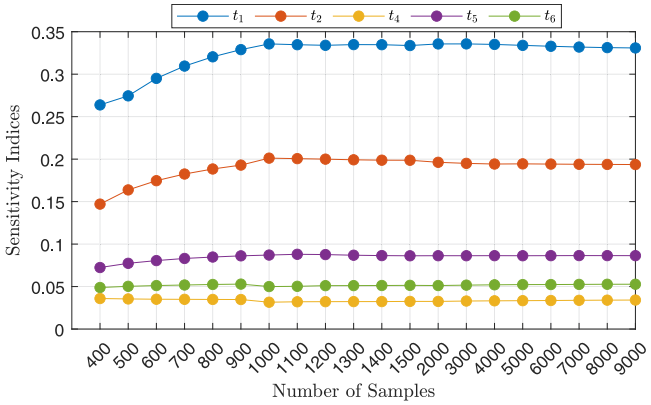

Fig. 9. Plot showing sensitivity indices evaluated with respect to $\mathcal{MI}^4$ versus the number of samples used to perform the geometric moment-dependent sensitivity analysis.

5.2.1. Metric to measure correlation

To further analyse the effect of sensitivity of parameters with respect to geometric moments and to compare it versus the sensitivity indices to that obtained for C_w, we introduce two metrics as below:

$$\text{NRMSE} = \frac{\sqrt{\sum_{i=1}^{n} \frac{\left(GSI_{T_i} - SI_{T_i}\right)^2}{n}}}{\max\left(\mathbf{SI}_T\right) - \min\left(\mathbf{SI}_T\right)} \tag{37}$$

$$\text{similarity} = \frac{\overline{\mathbf{SI}}_T \cdot \overline{\mathbf{GSI}}_T}{\|\overline{\mathbf{SI}}_T\| \, \|\overline{\mathbf{GSI}}_T\|} = \frac{\sum_i^n \overline{SI}_{T_i} \, \overline{GSI}_{T_i}}{\sqrt{\sum_i^n \overline{SI}_{T_i}} \sqrt{\sum_i^n \overline{GSI}_{T_i}}} \tag{38a}$$

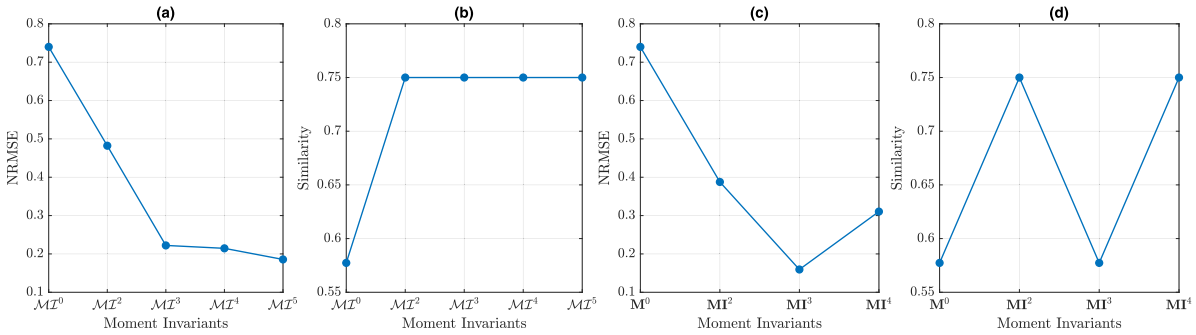

Fig. 10. Plot showing (a, c) NRMSE and (b, d) similarity values obtained using Eqs. (38) and (37) for $\mathcal{MI}^0$ to $\mathcal{MI}^5$ and $\mathbf{MI}^0$ to $\mathbf{MI}^4$ obtained for PD hull.

where

$$\overline{SI}_{T_i} = \begin{cases} 1 & \text{if } SI_{T_i} \geq \epsilon \\ 0 & \text{otherwise,} \end{cases} \qquad \overline{GSI}_{T_i} = \begin{cases} 1 & \text{if } GSI_{T_i} \geq \epsilon \\ 0 & \text{otherwise.} \end{cases} \tag{38b}$$

The first metric (Eq. (37)) is the normalised root mean squared error (NRMSE) which works directly on the sensitivity indices and measures the deviation between the two sets of sensitivity indices evaluated with C_w ($\mathbf{SI}_T$) and $\mathcal{MI}^s$ ($\mathbf{GSI}_T$). The second metric (Eq. (38)) is based on the cosine similarity, bounded between [0,1], which is used to measure the similarity between the parameters sensitive to $\mathcal{MI}^s$ and C_w. The perfect scenario will be that the parameters sensitive to C_w are also sensitive to $\mathcal{MI}^s$ or vice versa. Therefore, we measure the similarity on the two binary sensitivity vectors evaluated with C_w ($\overline{\mathbf{SI}}_T$) and $\mathcal{MI}^s$ ($\overline{\mathbf{GSI}}_T$) obtained with Eq. (38b). A sensitive parameter, i.e., a parameter with a sensitivity index greater than or equal to 0.05, gets a score of one, and an insensitive parameter gets zero. This is preliminary because we are not interested in the sensitivity indices; instead, we intend to categorise a parameter as sensitive or insensitive according to the sensitivity indices using the set threshold, ϵ.

Fig. 10(a, b) and Table 3 depict the NRMSE and similarity values obtained using Eqs. (37) and (38) for $\mathcal{MI}^0$, $\mathcal{MI}^2$, $\mathcal{MI}^3$, $\mathcal{MI}^4$ and $\mathcal{MI}^5$. From these figures, it can be seen that NRMSE achieves its maximum for $\mathcal{MI}^0$ and has a steep descent up to $\mathcal{MI}^3$. There is no significant difference between NRMSE of $\mathcal{MI}^3$ and $\mathcal{MI}^4$; however, it reduces slightly from 0.2146 to 0.1856 when sensitivity analyses are performed with $\mathcal{MI}^4$ and $\mathcal{MI}^5$. This is an apparent behaviour occurring as we increase the order of SSV by adding high-order geometric moments. The sensitivity indices of the parameters become closer to the sensitivity indices obtained with C_w. As mentioned earlier, sensitive parameters identified by $\mathcal{MI}^2$, $\mathcal{MI}^3$, $\mathcal{MI}^4$ and $\mathcal{MI}^5$ are the same, i.e., in all three cases, there is a 0.75 (or 75%) similarity between the sensitive parameters of SSVs and C_w. This shows that adding higher-order moments to SSV can better capture the parametric sensitivities; however, the improvement is marginal.

So far, we have measured the sensitivity of the parameters using $\mathcal{MI}^s$, which contains all the geometric moments from up to *sth*-order. The question arises what would be the result if we use geometric moment invariants of a particular order to perform SA, i.e., if we measure sensitivity to $\mathbf{MI}^s$ which contains the moments of *sth*-order only. The results of this experiment are shown in terms of NRMSE and similarity in Fig. 10(c) and (d), respectively. At $\mathbf{M}^0$, NRMSE is the highest, and similarity is the lowest. These values are equal to the case when $\mathcal{MI}^0$ is used as $\mathcal{MI}^0 = \mathbf{M}^0$ due to the reason mentioned earlier in Section 3.2. When $\mathbf{MI}^2$ is used to measure the sensitivity of the parameters, interestingly, NRMSE is lower than $\mathcal{MI}^2$, and both have the same similarity to the sensitive parameters of C_w. Similarly, NRMSE obtained with $\mathbf{MI}^3$ is lower than the $\mathcal{MI}^3$; however, the similarity with sensitive parameters of C_w is only 57%, which is the same when $\mathcal{MI}^0$ is used. The NRMSE of sensitivity indices obtained with $\mathbf{MI}^4$ and C_w is 0.3103, which is higher than the ones obtained with $\mathcal{MI}^3$ and $\mathcal{MI}^4$; nevertheless, the similarity is the same as $\mathcal{MI}^4$. These results show fluctuations in the sensitivity indices when only $\mathbf{MI}^s$ are used. This is because for geometric moments to be used as a shape descriptor, the SSV should be composed of all the geometric moments up to a specific order [23].

Table 4
Local and transition sensitive parameters of PD hull with respect to C_w and $\mathcal{MI}^4$.

QoI	Sensitive parameters	NMSE	Similarity
C_w	t_5, t_6, t_7, t_{13}, t_{16}, t_{19}	–	–
$\mathcal{MI}^4$	t_5, t_6, t_{13}, t_{16}, t_{19}	0.1296	91%

5.2.2. Sensitivity analysis while excluding most dominating sensitive parameters

In this section we have so far observed that parameters t_1 and t_2 are the most sensitive parameters to C_w, $\mathcal{MI}^2$, $\mathcal{MI}^3$ and $\mathcal{MI}^4$, which, as indicated in Section 4.2.1, are semi-global in nature when it comes to their high impact on shape modification. Therefore, it will be interesting to see if we exclude (i.e., keep them fixed) these parameters and perform SA on the remaining 24 parameters with respect to $\mathcal{MI}^4$ and C_w. The results of this experimentation are shown in Fig. 11(a).

There is a couple of noteworthy remarks regarding these results. First of all, there are six and five parameters, [t_5, t_6, t_7, t_{13}, t_{16}, t_{19}] and [t_5, t_6, t_{13}, t_{16}, t_{19}] sensitive to C_w and $\mathcal{MI}^4$, respectively, with $\epsilon \geq 0.05$. In the case of C_w, parameter, t_{19}, is the most sensitive one, followed by t_6. Note that out of these parameters, t_6 and t_{19}, are also sensitive when SA is performed with all 26 parameters; see in Fig. 7 and Table 4. It is noteworthy that in this case, t_{19} is a third sensitive parameter to $\mathcal{MI}^4$ and unlike the results in Fig. 7, it has significant sensitivity with the index value close to that of t_5 and t_6. Furthermore, apart from parameter t_7, all the remaining parameters sensitive to $\mathcal{MI}^4$ are also sensitive to C_w. Therefore, there is a high degree of similarity between sensitive parameters obtained with both quantities with similarity values equal to 0.9129 (91.29%) and NRMSE equal to 0.1296. This shows that by identifying more sensitive parameters with SSV, one can also fix the most dominating sensitive parameters and re-perform the sensitivity study as the computational cost of evaluating the moments is significantly less than evaluating C_w.

5.3. Sensitivity analysis for shape with simple geometry

As stated earlier in this section, selecting the order of SSV is influenced by the nature of problems' physics and geometry. It is reasonable to expect that for a simple geometry with fewer complex features, lower-order SSV would be sufficient for SA.

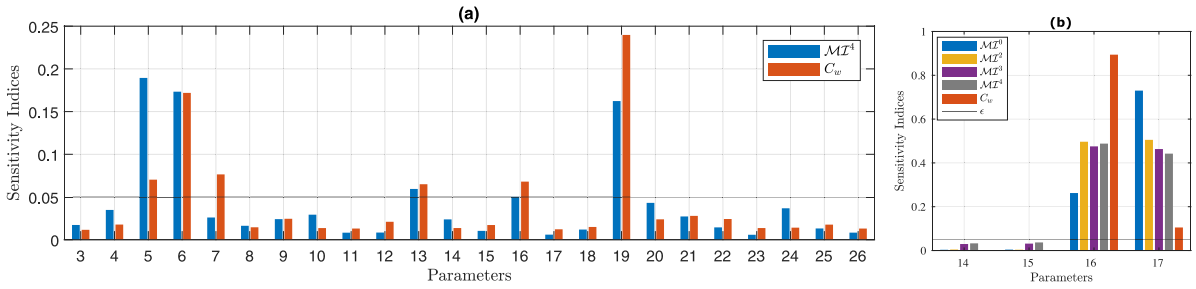

Fig. 11. Sensitivity indices obtained with sensitivity analysis preformed (a) with only local and transition parameters (t_3 to t_{26}) and (b) with only bow parameters (t_{14} to t_{17}) of PD hull using Eqs. (17) and (28) with respect to C_w and $\mathcal{MI}^s$, respectively.

To analyse this effect, we perform SA only for the parameters $[t_{14}, t_{15}, t_{16}, t_{17}]$ associated with the width, length, height and tip height of PD hull's bulbous bow. Compared to the overall hull form, the geometry of the bulbous bow is simple (mainly of elliptical type) but critical from the physical point of view. Sensitivity analyses are performed to measure the sensitivity of these parameters with respect to C_w and SSV, $\mathcal{MI}^s$ with $s = 0/2/3/4$ while fixing other parameters. The results of this experimentation are shown in Fig. 11(b). It can be seen that parameters $[t_{16}, t_{17}]$ sensitive to C_w with sensitivity indices greater than $\epsilon = 0.05$, are also sensitive to SSV of all orders. However, for $\mathcal{MI}^0$, the indices of t_{16} and t_{17} deviate largely from what obtained with respect to C_w. As order increases, the index of t_{16} increases whereas index of t_{17} decreases; getting closer to indices obtained with C_w. There is no significant difference between sensitivity indices obtained with respect to $\mathcal{MI}^2$, $\mathcal{MI}^3$ and $\mathcal{MI}^4$. Interestingly, in the case of $\mathcal{MI}^2$, $\mathcal{MI}^3$ and $\mathcal{MI}^4$, the sensitivity ranking of parameters is the same as obtained via C_w; thus, it gives similarity equal to 1.0000 (100%). The results of this experiment reveal that in the case of simple geometry, geometric moments of lower order are enough to capture parametric sensitivities associated with the local features of the hull.

5.4. Sensitivity analysis of DTMB hull model

As in the case of the PD hull, SA for the parameters of the DTMB hull commences with a 27-dimensional design space, which was sampled to create a dataset consisting of $N' = 9000$ samples. First, SA is performed to measure the sensitivity of parameters with respect to C_w, which is evaluated using the potential flow solver as described in Section 4.3. Afterwards, the covariance decomposition approach, along with Sobol's SA, is used to evaluate generalised total sensitivity indices for the parameters with respect to $\mathcal{MI}^0$, $\mathcal{MI}^2$, $\mathcal{MI}^3$ and $\mathcal{MI}^4$. As the objective here is to preliminary evaluate the parametric sensitivity using geometric moments, we first analyse results in terms of NRMSE and similarity, which are shown in Fig. 12(a) and (b), respectively. These results exhibit similar behaviour as the results in the case of the PD hull shown in Fig. 10(a) and (b). NMSE obtained with sensitivity indices of C_w and $\mathcal{MI}^0$ is the highest and decreases steadily up to $\mathcal{MI}^4$, with similar values when SA is performed with $\mathcal{MI}^2$ and $\mathcal{MI}^3$. Likewise, with the increase in the order of SSV, the similarity between the sensitive parameters obtained using C_w and geometric moments increases gradually from 0.1690 (16.90%) (evaluated with $\mathcal{MI}^0$) to 0.7715 (77.15%) (evaluated with $\mathcal{MI}^4$). One should recall that in the previous test case, the similarity value of 0.75 was consistent for $\mathcal{MI}^2$, $\mathcal{MI}^3$ and $\mathcal{MI}^4$, i.e., 75% of parameters sensitive to C_w were identified. However, in this test case, $\mathcal{MI}^2$ could only identify 66.81% of the parameters sensitive to C_w. Nevertheless, the similarity value achieved with $\mathcal{MI}^4$ for this test case is slightly higher than what was obtained for the PD Hull. This shows that also in this test case, $\mathcal{MI}^4$ achieves the highest similarity and lowest NRMSE to sensitivity indices of C_w, whereas $\mathcal{MI}^0$ shows the least similarity and highest NMSE. In conclusion, even for a test case like DTMB, whose parameterisation is not feature-driven, geometric moments can still significantly capture the sensitivity of parameters associated with physics. Summary of above discussed sensitivity results is provided in Table 5.

Table 5
Sensitive parameters of DTMB hull with respect to C_w and $\mathcal{MI}^s$ with $s = 0/2/3/4$.

QoI	Sensitive parameters	NMSE	Similarity
C_w	$t_4, t_8, t_{14}, t_{15}, t_{17}, t_{22}, t_{26}$	–	–
$\mathcal{MI}^0$	$t_9, t_{22}, t_{23}, t_{25}, t_{26}$	0.3984	17%
$\mathcal{MI}^2$	$t_3, t_4, t_8, t_9\ t_{14}, t_{15}, t_{24}, t_{26}$	0.1964	69%
$\mathcal{MI}^3$	$t_4, t_8, t_9\ t_{14}, t_{15}, t_{22}, t_{26}$	0.1868	77%
$\mathcal{MI}^4$	$t_4, t_8, t_9\ t_{14}, t_{15}, t_{22}, t_{26}$	0.1366	77%

Fig. 12(c) shows the sensitivity indices of the 27 design parameters obtained with respect to C_w and $\mathcal{MI}^4$. It can be seen that for C_w, 7 out of the 24 parameters, $[t_4, t_8, t_{14}, t_{15}, t_{17}, t_{22}, t_{26}]$, have a sensitivity index greater than ϵ and thus can be regarded as the most sensitive parameters with respect to C_w. Among these parameters, t_{14}, t_8 and t_{15} have substantially high sensitivity index while t_{17}, t_{22} and t_{26} have a sensitivity index close to $\epsilon = 0.05$. In case of $\mathcal{MI}^4$, there are 6 parameters, $[t_4, t_8, t_9\ t_{14}, t_{15}, t_{22}, t_{26}]$, with sensitivity index higher than 0.05. It is interesting to note that, except parameter t_9, parameters sensitive to $\mathcal{MI}^4$ are also sensitive to C_w. More importantly, the parameters, t_4, t_{14}, t_8 and t_{15}, are the top 4 sensitive parameters with respect to both C_w and $\mathcal{MI}^4$.

5.5. Composite geometric moment invariants

For complex geometries containing many features, SSV may require to include high-order geometric moments to capture detailed information about the shape, mainly associated with local intrinsic features. However, as mentioned earlier, higher-order moments are sensitive to noise. Therefore, instead of evaluating higher-order geometric moments for capturing detailed features, one may decompose the geometry into smaller segments whose geometries are simple enough to be represented easily with lower-order geometric moments. This will create a Composite-Shape-Signature Vector containing the geometric moment invariants up to *sth*-order for all shape segments and then use it to perform SA. In this connection, we shall henceforth refer to composite $\mathcal{MI}^s$ versus the global $\mathcal{MI}^s$ used in the previous section.

The segmentation of ship hulls used as test cases in the present work is shown in Fig. 13. Both hulls are divided into four parts: bow (bulbous bow for the PD hull and sonor dome for the DTMB

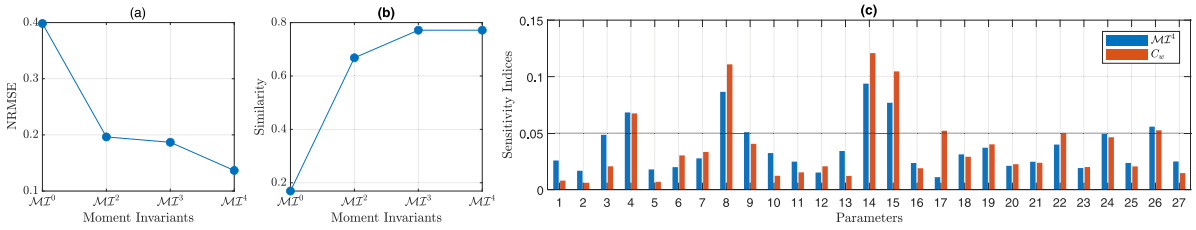

Fig. 12. Plot showing (a) NRMSE and (b) sensitivity values obtained using Eqs. (38) and (37) for $\mathcal{MI}^0$ to $\mathcal{MI}^4$ obtained for DTMB hull. (c) Sensitivity indices of DTMB hull's 27 design parameters obtained using Eqs. (17) and (28) with respect to C_w and $\mathcal{MI}^4$, respectively.

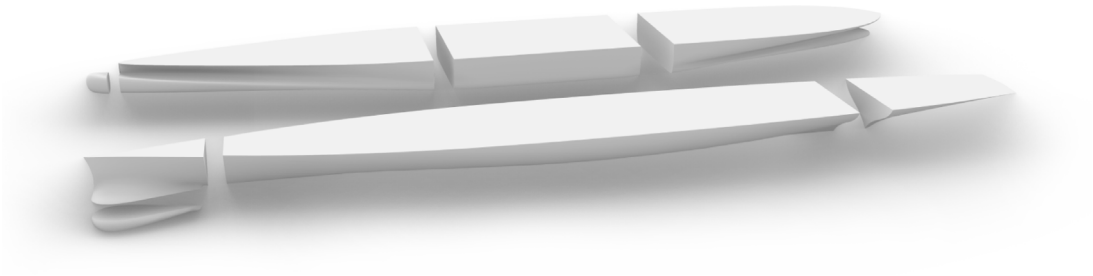

Fig. 13. Shape segmentation of PD and DTMB hulls used for sensitivity analysis performed with composite $\mathcal{MI}^5$.

hull), forward, mid-body, and aft segments. This segmentation is relatively easy for ship hulls and widely adopted in the literature. However, for other shapes, one can perform the segmentation based on the visible features or use an automatic segmentation method similar to one presented in [76]. After the segmentation, $\mathcal{MI}^4$ is evaluated, and the multivariate SA is performed, whose sensitivity results, along with C_w, are shown in Figs. 14 and 15 for PD hull and DTMB hull, respectively. The set of sensitive parameters of both hulls with respect to composite-$\mathcal{MI}^4$ are provided in Table 6. We shall first comment on the sensitivity results of the PD hull obtained with composite $\mathcal{MI}^4$ and compare them with the sensitivity results of global $\mathcal{MI}^4$ evaluated for the entire shape, given in Fig. 7. In this case, sensitivity results for C_w are the same as previously presented; however, the sensitivity of parameters to geometric moments changes due to the usage of composite $\mathcal{MI}^4$. From these results it can be seen that there are five parameters, $[t_1, t_2, t_5, t_6, t_{19}]$, sensitive to composite $\mathcal{MI}^4$ where, apart from t_{19}, the four remaining parameters are also sensitive with respect to global $\mathcal{MI}^4$. One should recall that in Fig. 7, t_{19} is the only parameter sensitive with respect to C_w but insensitive to global $\mathcal{MI}^4$. However, it is noteworthy that in the case of composite $\mathcal{MI}^4$, this parameter is sensitive with a substantial increment in its sensitivity index value. This results in the decline in NRMSE from 0.2145 (obtained with global $\mathcal{MI}^4$) to 0.1661 (obtained with composite $\mathcal{MI}^4$) and increment in similarity from 0.75 (75%) to 0.8944 (89.44%). Moreover, in the case of composite $\mathcal{MI}^4$, the first two sensitive parameters have the same ranking as the ranking obtained with C_w. This again shows the usability of geometric moments to perform reliable global SA.

Similar to the PD hull, interesting and improved results (shown in Fig. 15) are obtained when SA are performed for DTMB hull with composite $\mathcal{MI}^4$. In this case, instead of 7 we have 6 sensitive parameters, $[t_4, t_8, t_{14}, t_{15}, t_{22}, t_{26}]$. All the parameters sensitive to composite $\mathcal{MI}^4$ are also sensitive with respect to C_w. Furthermore, now the similarity between two sets of sensitive parameters increases from 0.7715 (77.15%) to 0.9258 (92.58%) and only one parameter, t_{17}, could not be categorised sensitive with respect to the composite $\mathcal{MI}^4$. The parameters t_9 and t_{24} are sensitive with respect to global $\mathcal{MI}^4$ and insensitive with respect to composite $\mathcal{MI}^4$ with significant reduction in their sensitivity indices. Furthermore, the parameter t_{22} is sensitive with respect to composite $\mathcal{MI}^4$ and C_w, but is insensitive with respect to global $\mathcal{MI}^4$ (see results in Fig. 12(c)). Therefore, NRMSE reduces from 0.1366 to 0.1301.

Table 6
Sensitive parameters of PD and DTMB hulls with respect to composite-$\mathcal{MI}^4$.

QoI	Sensitive parameters	NMSE	Similarity
Composite-$\mathcal{MI}^4$	PD hull $t_1, t_2, t_5, t_6, t_{19}$ DTMB hull	0.1661	89%
Composite-$\mathcal{MI}^4$	$t_4, t_8, t_{14}, t_{15}, t_{22}, t_{26}$	0.1301	93%

5.6. Selection of SSV's order to commence SA

From the above experimentation, it can be concluded that selecting the right order of SSV can be based on the complexity of the shape's geometry. For a geometry with fewer complex features, it would be sufficient to work with lower-order SSV, e.g., of order 2 or 3. On the contrary, complex geometries with many features may require SSV to include high-order geometric moments (e.g., of order ≥ 4) to capture detailed information about the shape, mainly associated with local intrinsic features. However, the higher-order moments can be sensitive to noise acquisition [25]. Therefore, instead of evaluating higher-order geometric moments for capturing detailed features, one could decompose the geometry into smaller segments whose geometries are simple enough to be represented easily with lower-order SSV. As a rule of thumb, *we recommend using 4th-order global-SSV for a simple geometry and 4th-order composite-SSV for complex geometry with many features.* This is also supported by the fact that various application areas, e.g., kinetic equations [74] and shape retrieval [56], use geometric moments up to the order of 4 and as shown in Section 5.2, with SSV of order higher than 4 only a marginal improvement can be excepted. The above discussion on the selection of the right order of SSV in relation to geometry complexity also aligns with the result of experiments performed in Sections 5.2 and 5.3. For instance, in the case of PD hull, only composite-SSV could categorise parameter, t_{19}, related to local feature like bulbous bow as sensitive; see Figs. 7, 8 and 14 for comparison. In contrast, for a bulbous bow, whose geometry type

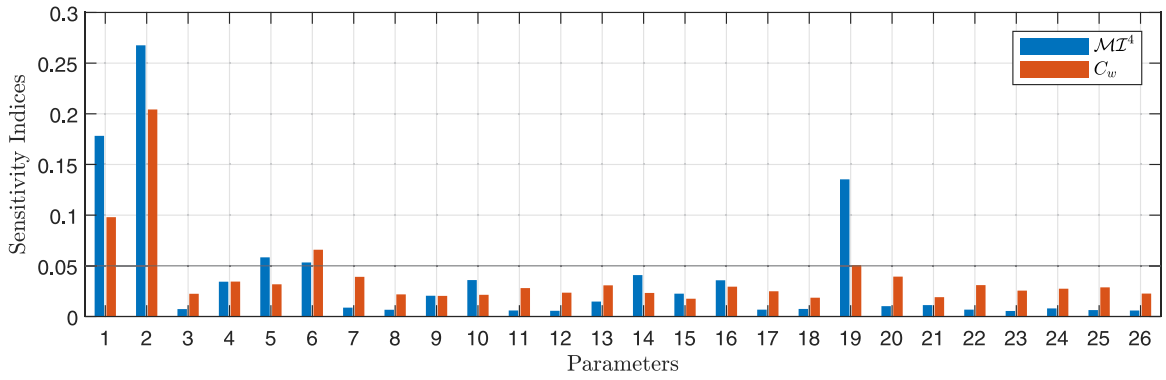

Fig. 14. Sensitivity indices of PD hull's 26 design parameters obtained using Eqs. (17) and (28) with respect to C_w and composite $\mathcal{MI}^4$, respectively.

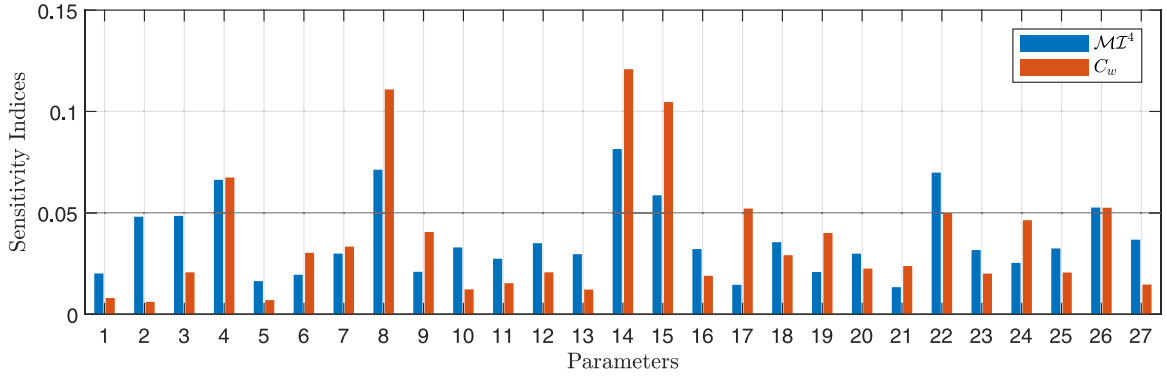

Fig. 15. Sensitivity indices of DTMB hull's 27 design parameters obtained using Eqs. (17) and (28) with respect to C_w and composite $\mathcal{MI}^4$, respectively.

is simple compared to the overall hull form, the global-SSV of 2nd-order was enough to capture the parametric sensitives; see Fig. 11(b).

5.7. Summary of sensitivity results

Before proceeding to the last part of this section, which will exploit our SA approach for shape optimisation, we offer the reader a summary of the sensitivity results obtained:

1. For both the PD and DTMB hulls, the NRMSE between sensitivity indices evaluated with respect to C_w and $\mathcal{MI}^s$ reduces with the increment in s.
2. Similarity between the parameter sensitivities with respect to C_w and $\mathcal{MI}^s$ increases with respect to s up to $s = 3$ but no significant improvement is observed when $s = 4$.
3. In comparison to global $\mathcal{MI}^s$, the composite $\mathcal{MI}^s$ captures better parametric sensitivities.
4. The results in Figs. 7 and 11 show that out of the 26 parameters that control the parametric modeller of PD, 7/8 parameters are significantly sensitive with respect to $\mathcal{MI}^4/C_w$, respectively (see Table 7).
5. A similar behaviour is observed from Figs. 12 and 15 for the DTMB hull: 7/6 parameters out of the 27 parameters are sensitive with respect to $\mathcal{MI}^4/C_w$, respectively (see Table 7).
6. The similarity between the subsets of significantly sensitive parameters with respect to C_w and $\mathcal{MI}^4$ is 79.06% for the PD hull and 92.58% for the DTMB hull.
7. In the case of PD (DTMB) hull, the SA with respect to $\mathcal{MI}^4$ helps to achieve a 73.08% (74.07%) reduction in the dimension of the design space.

Table 7
Summary of the sensitivity analysis results obtained from the previously discussed experimentation.

	Sensitive parameters	Similarity
	With respect to C_w	
PD hull	$t_1,\ t_2,\ t_5,\ t_6,\ t_7,\ t_{13},\ t_{16},\ t_{19}$	–
DTMB hull	$t_4,\ t_8,\ t_{14},\ t_{15},\ t_{22},\ t_{26}$	–
	With respect to $\mathcal{MI}^4$	
PD hull	$t_1,\ t_2,\ t_5,\ t_6,\ t_{13},\ t_{16},\ t_{19}$	79.06%
DTMB hull	$t_4,\ t_8,\ t_{14},\ t_{15},\ t_{17},\ t_{22},\ t_{26}$	92.58%

5.8. Shape optimisation

One of the key objectives of extracting parametric sensitivities is to achieve rapid design improvements already at the preliminary stage of shape optimisation. In this connection, once the subset $\mathbf{t}_{\mathcal{MI}}$ of parameters sensitive to $\mathcal{MI}^4$ is selected from the original parametric set $\mathbf{t}$, we use them to construct a design space $\mathcal{X}_{\mathcal{MI}}$ of lower dimension to expedite the shape optimisation performed against physical QoI, i.e., C_w. For the PD and DTMB hulls, their sensitive parameters $\mathbf{t}_{\mathcal{MI}} = \{t_1, t_2, t_5, t_6, t_{13}, t_{16}, t_{19}\}$ and $\mathbf{t}_{\mathcal{MI}} = \{t_4, t_8, t_{14}, t_{15}, t_{17}, t_{22}, t_{26}\}$ create two 7-dimensional design spaces ($\mathcal{X}_{\mathcal{MI}}$). As stated earlier that typically parametric sensitivities are learnt directly with physical QoI, which can be extensively computational demanding due to the need of performing physical analysis for both SA and shape optimisation. To experimentally prove the potential of moments for learning parametric sensitivities to aid optimisation, we construct a reduced-dimension design space $\mathcal{X}_{c_w}$ with the subset $\mathbf{t}_{c_w}$ of parameters sensitive to C_w. The shape optimisation is performed in $\mathcal{X}_{\mathcal{MI}}$ and $\mathcal{X}_{c_w}$ with an objective to minimise their C_w.

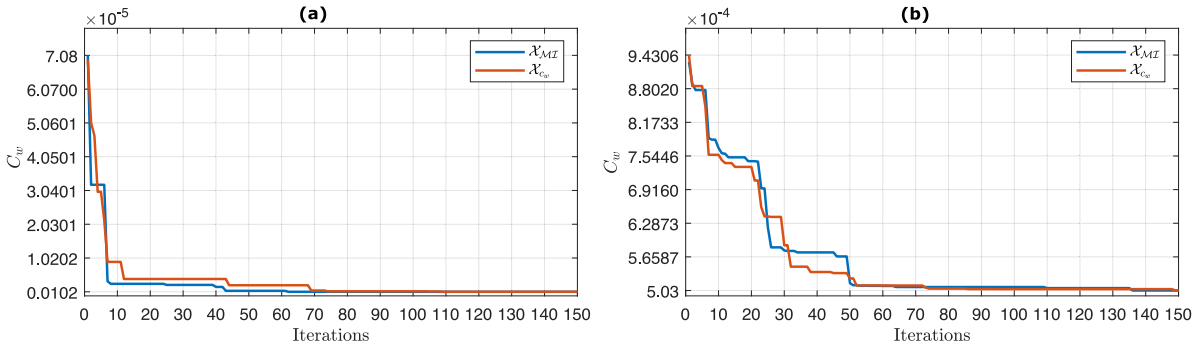

Fig. 16. Plot showing C_w versus optimisation iterations performed to optimise (a) PD and (b) DTMB hulls in $\mathcal{X}_{\mathcal{MI}}$ and $\mathcal{X}_{c_w}$.

Table 8
C_w values of optimal designs obtained when optimisation is performed in $\mathcal{X}_{\mathcal{MI}}$ and $\mathcal{X}_{c_w}$ for PD and DTMB hulls.

Runs	C_w						
	#1	#2	#3	#4	#5	Average	STD
Design space	PD hull						
$\mathcal{X}_{\mathcal{MI}}$	1.0328E−07	1.0395E−07	1.0244E−07	**1.0205E−07**	1.0505E−07	1.0335E−07	1.2013e−09
$\mathcal{X}_{c_w}$	1.0304E−07	1.0318E−07	1.0355E−07	1.0303E−07	**1.0302E−07**	1.0316E−07	2.2546e−10
	DTMB hull						
$\mathcal{X}_{\mathcal{MI}}$	5.0809E−04	5.0945E−04	5.1097E−04	**5.0314E−04**	5.1419E−04	5.0917E−04	3.6349E−06
$\mathcal{X}_{c_w}$	5.0455E−04	5.0455E−04	**5.0269E−04**	5.0616E−04	5.0440E−04	5.0447E−04	1.09891E−06

The parametric modellers [4,27] used in this work ensure the generation of valid geometries, i.e., the possibility of generating disjoint and self-intersecting surfaces is negligible. However, a valid geometry may be unrealistic or impractical; therefore, our optimisation in Eq. (1) can be reformulated based on the set of design constraints as:

Optimisation:

$$\begin{aligned} &\text{Find } \mathbf{t}^*_{\mathcal{MI}} \in \mathbb{R}^m \quad \text{such that} \\ &\quad C_w(\mathbf{t}^*_{\mathcal{MI}}) = \min_{\mathbf{t}_{\mathcal{MI}} \in \mathcal{X}_{\mathcal{MI}}} C_w(\mathbf{t}^*_{\mathcal{MI}}) \\ &\text{subject to} \quad 0.95V_0 \le V(\mathbf{t}_{\mathcal{MI}}) \le 1.05V_0, \\ &\qquad\qquad 0.95Bwl_0 \le Bwl(\mathbf{t}_{\mathcal{MI}}) \le 1.05Bwl_0, \\ &\qquad\qquad Lwl(\mathbf{t}_{\mathcal{MI}}) = Lwl_0, \\ &\qquad\qquad T(\mathbf{t}_{\mathcal{MI}}) = T_0. \end{aligned} \tag{39}$$

Here, $\mathbf{t}_{\mathcal{MI}}$ is a subset of sensitive parameters obtained with respect to moment and $\mathcal{X}_{\mathcal{MI}}$ is the corresponding design space, whose dimension is less than the original space ($\mathcal{X}$). V, B_{WL}, L_{WL}, T correspond to volume, length and beam at the waterline, and draft, respectively. The sub-index $(\cdot_0)$ indicates the quantity values for the baseline hull design. These constraints focus on exploring an optimal design whose key features reside in the vicinity of the baseline design. Therefore, the resulting optimal design is considered practical as the baseline design.

The optimisation is performed using the Jaya Algorithm (JA) [77], with the objective to minimise C_w. JA is a simple yet effective stochastic meta-heuristic optimisation technique whose performance has been proven in various engineering applications. JA may provide different results in each run; therefore, five different optimisation runs are performed in the present work. In each run, a total of 150 iterations are conducted. Table 8 shows the C_w values obtained at the 150th iteration of shape optimisation performed in $\mathcal{X}_{c_w}$ and $\mathcal{X}_{\mathcal{MI}}$) for PD and DTMB hulls, along with the average C_w in all five runs. From this table, it can be seen that in the case of the PD hull, the best design is obtained at the fourth and fifth run from $\mathcal{X}_{\mathcal{MI}}$ and $\mathcal{X}_{c_w}$ with C_w equal to 1.0205E−07 and 1.0302E−07, respectively. Fig. 16(a) shows C_w values in all 150 iterations for these two runs. It is noteworthy that the optimal design obtained from $\mathcal{X}_{\mathcal{MI}}$ has better performed (i.e., its C_w value is less) compared to the design obtained from $\mathcal{X}_{c_w}$. However, on average, the C_w obtained from $\mathcal{X}_{\mathcal{MI}}$ with fives run at their 150th iteration is slightly higher, with C_w equal to 1.0335E−07, compared to the design obtained from $\mathcal{X}_{c_w}$, which is equal to 1.0316E−07. The optimal designs obtained for the PD hull from this shape optimisation experiment are shown in Fig. 17. Fig. 17(a) and (b) compare the baseline and optimal designs obtained from $\mathcal{X}_{\mathcal{MI}}$ and $\mathcal{X}_{c_w}$ in terms of their cross-sections (bodyplan) while Fig. 17(c) show this comparison between the two optimal designs.

Fig. 17(d–f) show the intensity of deviation between the features of these designs as a heat map plotted using the one-sided Hausdorff Distance (H_d) between two objects and features with maximum deviation ($H_d = 1$) are highlighted in red. Similar features are highlighted in dark blue when $H_d = 0$. From these results, it can be seen that the design optimised from $\mathcal{X}_{c_w}$ has maximum deviation at the forward part of the hull, and the design optimised from $\mathcal{X}_{\mathcal{MI}}$ show maximum deviation from the baseline design at the aft segment. These slight geometric dissimilarities between the two optimised hulls (see Fig. 17(c) and (f)) are due to the existence of one extra parameter (t_7) in $\mathbf{t}_{c_w}$, which, as shown in Fig. 4, modifies the rise of the forward part of hull's flat-of-side. Nevertheless, in terms of performance, there is no significant difference between two hulls; i.e., the C_w of optimised hulls in Fig. 17(a) and (b) obtained with $\mathbf{t}_{c_w}$ and $\mathbf{t}_{\mathcal{MI}}$ is 1.2976E−07 and 1.0328E−07, respectively. The C_w value of the baseline PD hull (shown in Fig. 2(a)) is 1.07E−04, which is higher than the optimal designs obtained from both sensitive design spaces. This shows that one can achieve significant improvement in the design using sensitive parameters only.

Fig. 16(b) shows the C_w values over 150 iterations during the fourth and fifth optimisation run for the DTMB hull performed in $\mathcal{X}_{\mathcal{MI}}$ and $\mathcal{X}_{c_w}$ created for DTMB hull. From the results in Fig. 16(b) and Table 8 it can be seen that, like in the case of PD hull, the optimal design obtained in $\mathcal{X}_{\mathcal{MI}}$ has also lower C_w value compared to the design obtained from $\mathcal{X}_{c_w}$. These values are notably less than that of the baseline design of DTBM hull in Fig. 2(b), which is equal to 1.05E−03. Moreover, for this

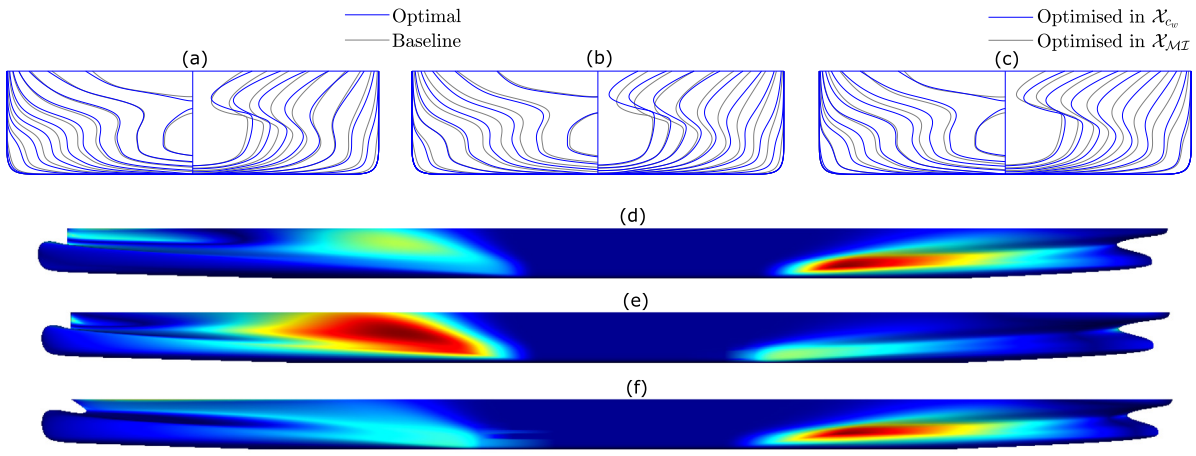

Fig. 17. Comparison between the baseline and optimised PD hulls obtained from $\mathcal{X}_{\mathcal{MI}}/\mathcal{X}_{c_w}$ in terms of (a)/(b) bodyplans and (d)/(e) one-sided Hausdorff Distance, respectively. Similar comparison between optimised designs of $\mathcal{X}_{c_w}$ and $\mathcal{X}_{\mathcal{MI}}$ in terms of (c) bodyplans and (f) one-sided Hausdorff Distance. (For interpretation of the references to colour in this figure legend, the reader is referred to the web version of this article.)

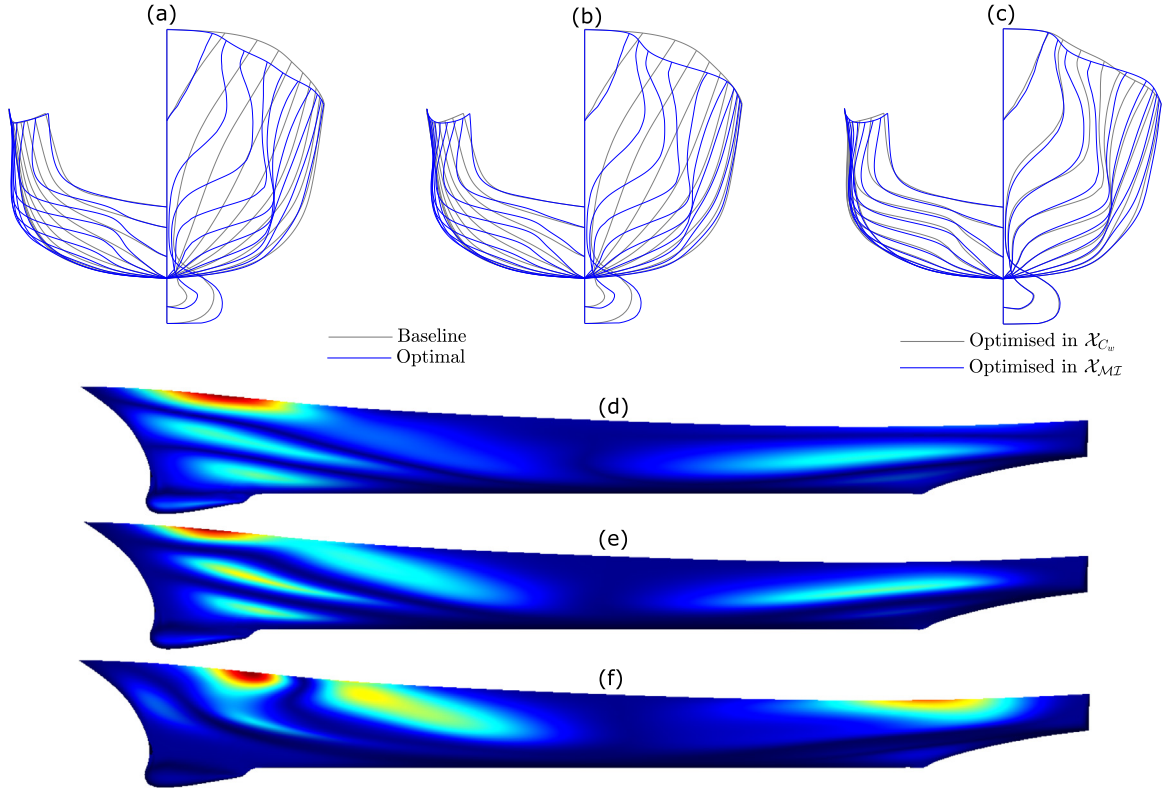

Fig. 18. Comparison between the baseline and optimised DTMB hulls obtained from $\mathcal{X}_{\mathcal{MI}}/\mathcal{X}_{c_w}$ in terms of (a)/(b) bodyplans and (d)/(e) one-sided Hausdorff Distance, respectively. Similar comparison between optimised designs of $\mathcal{X}_{c_w}$ and $\mathcal{X}_{\mathcal{MI}}$ in terms of (c) bodyplans and (f) one-sided Hausdorff Distance.

hull, the average C_w value of five optimisation runs, shown in Table 8, is 5.0917E−04 when optimisation is performed in $\mathcal{X}_{\mathcal{MI}}$, which, unlike the case of PD hull, is slightly higher then average C_w (equal to 5.0447E−04) obtained from $\mathcal{X}_{c_w}$. The percentage difference between the two values is 0.92%, which is negligible. The comparison between the optimal and baseline design of the DTMB hull is shown in Fig. 18 in terms of the bodyplan and the Hausdorff distance heat map. The map in Fig. 18(d) shows that in the case of $\mathcal{X}_{\mathcal{MI}}$ the maximum deviation of the optimal design from the baseline occurs close to the waterline at the mid-body segment of the hull. In contrast, the design optimised from $\mathcal{X}_{c_w}$ deviates notably from the baseline design at the forward segment close to the entrance of the hull; Fig. 18(e). On the other hand, comparing the two optimised in Fig. 18(c) and (f) one can observe a similar behaviour as the PD hull in terms of geometric variation. For the DTMB hull, parameters sensitive to C_w and $\mathcal{MI}^4$ are $\mathbf{t}_{\mathcal{MI}} = \{t_4, t_8, t_{14}, t_{15}, t_{17}, t_{22}, t_{26}\}$ and $\mathbf{t}_{c_w} = \{t_4, t_8, t_{14}, t_{15}, t_{22}, t_{26}\}$ and again, apart from t_{17}, parameters sensitive to both sets are the same. However, geometric variation

Table 9
C_w values and the percentage improvement in baseline design of PD and DTMB hulls made when shape optimisation is performed in sensitive (($\mathcal{X}_{\mathcal{MI}}$ and $\mathcal{X}_{c_w}$)) and original ($\mathcal{X}$) design spaces.

	Baseline design	Design from $\mathcal{X}_{c_w}$	Design from $\mathcal{X}_{\mathcal{MI}}$	Design from $\mathcal{X}$
	PD hull			
C_w	1.0678E−04	1.0302E−07	1.0205E−07	1.05081E−07
	DTMB hull			
C_w	1.0531E−03	5.0269E−04	5.0314E−04	8.9218E−05

between two optimised DTMB hulls is slightly higher compared to PD hulls. However, despite the design difference both optimised designs have similar performance, e.g., their C_w is equal to 5.0269E−04 and 5.0314E−04.

The above results indicate that for both PD and DTMB hulls, the optimal designs obtained from $\mathcal{X}_{\mathcal{MI}}$ and $\mathcal{X}_{c_w}$ have similar performance in terms of the wave resistance C_w. Even with only seven sensitive parameters for the PD hull and six sensitive parameters for the DTMB hull in $\mathcal{X}_{\mathcal{MI}}$, a substantial improvement is made versus the baseline designs in terms of C_w. Table 9 summarises C_w values of the parent and optimal designs obtained from sensitive ($\mathcal{X}_{\mathcal{MI}}$ and $\mathcal{X}_{c_w}$) and original ($\mathcal{X}$) design spaces. This shows that the biggest improvement for the PD hull is achieved when shape optimisation is performed with sensitive parameters instead of using the entire set of 26 design space parameters. These impaired optimisation results obtained from $\mathcal{X}$ can be attributed to its high dimensionality. As $\mathcal{X}$ is 27-dimensional for the PD hull, optimisation exhibits slow convergence, requiring more design evaluations, which results in a higher computational cost. Furthermore, more than half of the improvement made to the DTMB design achieved with a full set of 27 design parameters of the DTMB hull is contributed by only six parameters sensitive to $\mathcal{MI}^4$.

5.9. Computational cost

The computational cost to perform SA to geometric moments is glaringly less than performing SA with $\mathcal{X}_{c_w}$ and $\mathcal{X}_{\mathcal{MI}}$. On a PC with Intel(R) Xeon(R) Gold 6226 CPU with 2.70 GHz and 2.69 GHz processors and 128 GB of memory on average, it takes 11.552 and 9.039 s to evaluate the fourth-order shape-signature vector ($\mathcal{MI}^4$) for the PD and DTMB hull geometries composed of triangulated meshes with 1,968,835 and 2,512,886 vertices, respectively. For the PD and DTMB hulls, IGA-BEM and potential flow solvers take approximately 86.505 and 69.297 s to evaluate C_w. Consequently, for the PD hull, the overall computational cost for performing SA with respect to global $\mathcal{MI}^4$ and C_w is 29.0154 and 216.2701 h, respectively. Similarly, the computational cost for performing SA for DTMB hull with respect to C_w is also significantly high. Therefore, this proves that performing SA via geometric moments can provide a prior estimation of the parameters' sensitivity with extensively reduced computational cost.

5.10. Limitation of geometric moment invariants for sensitivity analysis

So far, in this section, we have demonstrated that SSV composed of geometric moment invariants up to fourth-order are capable of revealing parametric sensitivities for both test cases. However, despite their usefulness to expedite SA, moments can only be used for physical quantities, with tight coupling with the geometry, such as C_w. In general, an experienced designer/engineer can easily identify the dependence of a physical quantity on geometry, thereby on moments. Therefore, one can make a technically sound judgement on using geometric moments to preliminary drive the sensitivity of the parameters for their problem. Our use of geometric moments is based on the fact that, like most physical quantities, moments are sensitive to the variation of shape features, and the sensitive parameters are those with a high effect on the shape and thus on the associated physics. However, it is not unlikely that some parameters may have a high impact on the shape but a negligible impact on the physics in a design problem. In that case, one may require SSV composed of geometric moments of higher than fourth-order. For these reasons, moments may not be able to scale well versus other physical quantities as they did in the present case, especially for black-box problems or problems with no strong dependence of physical QoI on moments, such as it is the case of frictional resistance of the hull. Thus, a good understanding of the underlying physics is necessary to perform a geometric-moment dependent SA. In addition, moments can only be used for the SA of 2D/3D design problems. In contrast, SA is also widely used in the context of numerical problems with no geometrical objects/domains like [16,46].

Nevertheless, there exist a wide variety of problems [6,20,21,23–25,50] for which performing geometric-moment dependent SA can be very beneficial to reduce the computational cost of working directly with the physics. Moreover, as discussed in Section 4, our methodology is based on two pillars:

- The collocation BEM for Fredholm Boundary Integral Equations (BIE) of the second type, used for formulating and solving the elliptical exterior boundary-value problem (BVP) associated with the chosen QoI. Along with the Galerkin Finite-Element Method (FEM), collocation BEM provides a standard weak formulation for solving various problems in continuum mechanics and is especially suitable for BVP's defined on infinite domains, which is exactly the case for the wave-resistance problem.
- A pair of parametric modellers (PD [27] and DTMB [4]), capable to parametrise in robust and efficient manner complex free-form objects.

Based on the above remarks, we believe that the proposed approach can be applied to a broader class of shape optimisation problems that can be modelled via BIE on free-form geometries. Even if there is no strong connection of physics under consideration with geometric moments, they can at least capture the sensitivity of parameters to shape variation in a pure geometrical setting. This can be very useful at the preliminary stage design stage of constructing a parametric model, where the decision on type and dimensionality of parameterisation is made based on the effect a parameter can have on the original shape. This is related to the previously mentioned fact that designers are interested in parameterisation at the initial design stage, which can deliver the highest variability possible. This is especially of interest for parametric generative design [78,79].

Despite the limitations mentioned above, the results presented herein support the assertion that at least in the field of naval architecture, ocean and marine engineering, where these techniques are widely used, the proposed approach constitutes a valuable contribution. Furthermore, our end aim is to find a class of

design problems specifically in maritime and aeronautical fields, where these approaches are extensively used and ultimately, to trigger an interest in the research community towards exploring such physics-correlated but computationally inexpensive quantities to perform SA as a priori for identifying the sensitivity of parameters.

6. Conclusion and future works

This work describes our quest to support computationally demanding physical models with the aid of efficient geometric quantities such as geometric moments and their invariants. Using such geometric quantities, we proposed a method to expedite Sensitivity Analysis (SA) in the context of shape optimisation of 3D free-form shapes such as ship hulls. Our choice of geometric moments is based on the fact that they are intrinsic properties of solid shapes' underlying geometry that can provide essential design indications to facilitate designers in CAD. The set of geometric moment invariants up to particular order can also be used to create a shape-signature vector, which approximates the shape as order increases. Moreover, computing geometric moments is also vital for physics-based simulations that help in improving realism in physical animations. To prove that geometric moments can benefit designers as a prior check on the sensitivity of parameters, we utilised wave-resistance coefficient (C_w) as a physical quantity, as it is a crucial design consideration for a ship hull design towards improving efficiency and thus decreasing Fuel Oil Consumption. The distribution of the hulls' geometry, especially longitudinally, has a similar impact on geometric moments as C_w. To validate our claim, we utilised two different hull models, PD and DTMB hulls, which are constructed, parameterised and physically evaluated with two different approaches. Various experiments are performed with varying degrees of both global and composite shape-signature vectors and C_w to experimentally quantify the degree of similarity between the parameters sensitive to these quantities. The results from these experiments revealed a good correlation between the sensitive parameters obtained from the fourth-order composite shape-signature vectors ($\mathcal{MI}^s$) and C_w. In the case of the PD hull, seven parameters sensitive to $\mathcal{MI}^4$ are also among the 8 parameters sensitive to C_w. Interestingly, similar results are obtained for the DTMB hull, where 6 out of 7 sensitive parameters to C_w are also sensitive to $\mathcal{MI}^4$. Afterwards, two different design spaces are constructed for both hull models, one with sensitive parameters obtained with C_w and the other with $\mathcal{MI}^s$. Shape optimisation is performed in both spaces performed via a meta-heuristic optimisation approach. Final optimisation results showed that the design generated from design space constructed with sensitive parameters of C_w and $\mathcal{MI}^4$ for both types of hulls offer similar performance; however, interestingly, the optimal hull designs from $\mathcal{MI}^4$ have sightly better performance.

In future work, our prime aim is to explore other computationally demanding engineering design problems for which geometric moments can aid parametric analysis, specifically intra-sensitivity analysis [10]. Moreover, we are also interested in exploring other shape integral properties along with their usage to support surrogate and reduced-order modelling, specifically in the context of physics-informed learning [14].

CRediT authorship contribution statement

Shahroz Khan: Conceptualization, Methodology, Software, Experimentation, Visualization Writing – original draft, Writing – review & editing. **Panagiotis Kaklis:** Conceptualization, Methodology, Supervision, Validation, Funding acquisition, Writing – review & editing. **Andrea Serani:** Validation, Software – Parametric Modelling and Analysis of DTMB Hull, Writing – review & editing. **Matteo Diez:** Conceptualization, Funding acquisition, Writing – review & editing.

Declaration of competing interest

The authors declare that they have no known competing financial interests or personal relationships that could have appeared to influence the work reported in this paper.

Acknowledgements

The first two authors are thankful for the support and funding received from the EU Horizon-2020 Research and Innovation Programme under the Marie Skłodowska-Curie grant agreement No. 860843 – "*GRAPES: Learning, Processing and Optimising Shapes*". The third and fourth authors are grateful to the US Office of Naval Research Global for its support through grants N62909-11-1-7011 and N62909-21-1-2042. Furthermore, the authors thank Professor K. Kostas, Nazarbayev University (KZ), for providing free access to the PD hull parametric modeller and his tremendous and advice with the IGA-BEM solver.

Appendix. Moment computation

To start the computation of geometric moments of $\mathcal{G}$, let be given a vector field $\mathbf{f} : \mathbb{R}^n \to \mathbb{R}^3$ over $\mathcal{V}$, whose boundary is piece-wise smooth surfaces. The divergence theorem states that the volume integral of the divergence (div) of $\mathbf{f}$ over $\mathcal{V}$ equals the surface integral of the normal component $\hat{\mathbf{n}}$ of $\mathbf{f}$ over triangulation S, which can be formalised as

$$\operatorname{div}(\mathbf{f}) = \sum \frac{\partial f_i}{\partial t_i} \tag{A.1}$$

$$\int_V \operatorname{div}(\mathbf{f})\, \mathrm{dV} = \int_S \mathbf{f} \cdot \hat{\mathbf{n}}\, \mathrm{d}S. \tag{A.2}$$

With Eq. (A.2) we convert the volume integrals, which are difficult to evaluate, into surface integrals that are easy to evaluate over S. However, this theorem is only applicable if $\mathbf{f}$ is continuous and have continuous first partial derivatives in the region containing $\mathcal{V}$. To evaluate moments using this theorem, consider the following field:

$$\mathbf{f} = \frac{1}{3} x^p\, y^q\, z^r \left(\frac{x}{p+1}\hat{\mathbf{i}} + \frac{y}{q+1}\hat{\mathbf{j}} + \frac{z}{r+1}\hat{\mathbf{k}} \right). \tag{A.3}$$

and thus

$$M^{p,q,r}(\mathcal{G}) = \int_V \operatorname{div}(\mathbf{f})\, \mathrm{dV} = \sum_{i=1}^{N} \int_{T_i} \mathbf{f} \cdot \hat{\mathbf{n}}\, \mathrm{d}S_i, \tag{A.4}$$

where $\hat{\mathbf{n}}_i$ is the unit normal vector on the triangle T_i, which can be represented as a linear parametric surface as

$$S_i(u, v) = \boldsymbol{\alpha}_i u + \boldsymbol{\beta}_i v + \mathbf{c}_i, \quad (u, v) \in \Omega_i \subset \mathbb{R}^2, \tag{A.5}$$

here Ω_i can be taken to be the triangle with vertices $(0, 0)$, $(1, 0)$, $(0, 1)$. Then

$$M^{p,q,r}(\mathcal{G}) = \sum_{i=1}^{N} \int_{T_i} \mathbf{f} \cdot \hat{\mathbf{n}}_i \sqrt{\mathbf{E}_i \mathbf{G}_i - \mathbf{F}_i^2}\, \mathrm{d}u\mathrm{d}v, \tag{A.6}$$

where

$$\mathbf{E}_i = S_{i,u} \cdot S_{i,u} = |\boldsymbol{\alpha}_i|^2, \quad \mathbf{F}_i = S_{i,u} \cdot S_{i,v} = 0, \quad \mathbf{G}_i = S_{i,v} \cdot S_{i,v} = |\boldsymbol{\beta}_i|^2. \tag{A.7}$$

Here, $\mathbf{E}_i$, $\mathbf{F}_i$ and $\mathbf{G}_i$ are the constant first-order fundamental quantities of the S_i. Now, substituting Eq. (A.7) into Eg. (A.6) we get

$$M^{p,q,r}(\mathcal{G}) = \sum_{i=1}^{N} \int_{T_i} \mathbf{f} \cdot \hat{\mathbf{n}}_i \, |\boldsymbol{\alpha}_i| \, |\boldsymbol{\beta}_i| \, du dv \tag{A.8}$$

with

$$\hat{\mathbf{n}}_i = \frac{S_{i,u} \times S_{i,v}}{\sqrt{\mathbf{E}_i \mathbf{G}_i - \mathbf{F}_i^2}} = \frac{\boldsymbol{\alpha}_i \times \boldsymbol{\beta}_i}{|\boldsymbol{\alpha}_i| \, |\boldsymbol{\beta}_i|} \tag{A.9}$$

and

$$\mathbf{f}(x, y, z)|_{T_i} = \mathbf{f}\left(t_i(u, v), y_i(u, v), z_i(u, v)\right), \tag{A.10}$$

with $x_i(u, v)$, $y_i(u, v)$ and $z_i(u, v)$ are the x-, y- and z-components of $S_i(u, v)$.

References

[1] Schulz A, Xu J, Zhu B, Zheng C, Grinspun E, Matusik W. Interactive design space exploration and optimization for CAD models. ACM Trans Graph 2017;36(4):1–14. http://dx.doi.org/10.1145/3072959.3073688.

[2] Sun L, Gao H, Pan S, Wang J-X. Surrogate modeling for fluid flows based on physics-constrained deep learning without simulation data. Comput Methods Appl Mech Engrg 2020;361:112732. http://dx.doi.org/10.1016/j.cma.2019.112732.

[3] Serani A, Diez M, van Walree F, Stern F. URANS analysis of a free-running destroyer sailing in irregular stern-quartering waves at sea state 7. Ocean Eng 2021;237:109600. http://dx.doi.org/10.1016/j.oceaneng.2021.109600.

[4] D'Agostino D, Serani A, Diez M. Design-space assessment and dimensionality reduction: An off-line method for shape reparameterization in simulation-based optimization. Ocean Eng 2020;197:106852. http://dx.doi.org/10.1016/j.oceaneng.2019.106852.

[5] Khan S, Awan MJ. A generative design technique for exploring shape variations. Adv Eng Inform 2018;38:712–24. http://dx.doi.org/10.1016/j.aei.2018.10.005.

[6] Taber A, Kumar G, Freytag M, Shapiro V. A moment-vector approach to interoperable analysis. Comput Aided Des 2018;102:139–47. http://dx.doi.org/10.1016/j.cad.2018.04.026.

[7] Belibassakis K, Gerostathis TP, Kostas K, Politis C, Kaklis P, Ginnis A, Feurer C. A BEM-isogeometric method for the ship wave-resistance problem. Ocean Eng 2013;60:53–67. http://dx.doi.org/10.1016/j.oceaneng.2012.12.030.

[8] Masood Z, Khan S, Qian L. Machine learning-based surrogate model for accelerating simulation-driven optimisation of hydropower kaplan turbine. Renew Energy 2021;173:827–48. http://dx.doi.org/10.1016/j.renene.2021.04.005.

[9] Raissi M, Perdikaris P, Karniadakis GE. Physics-informed neural networks: A deep learning framework for solving forward and inverse problems involving nonlinear partial differential equations. J Comput Phys 2019;378:686–707. http://dx.doi.org/10.1016/j.jcp.2018.10.045.

[10] Khan S, Kaklis P. From regional sensitivity to intra-sensitivity for parametric analysis of free-form shapes: Application to ship design. Adv Eng Inform 2021;49:101314. http://dx.doi.org/10.1016/j.aei.2021.101314.

[11] Rios T, Sendhoff B, Menzel S, Bäck T, van Stein B. On the efficiency of a point cloud autoencoder as a geometric representation for shape optimization. In: 2019 IEEE symposium series on computational intelligence (SSCI). IEEE; 2019, p. 791–8. http://dx.doi.org/10.1109/SSCI44817.2019.9003161.

[12] Lukaczyk TW, Constantine P, Palacios F, Alonso JJ. Active subspaces for shape optimization. In: 10th AIAA multidisciplinary design optimization conference. 2014, p. 1171. http://dx.doi.org/10.2514/6.2014-1171.

[13] Kucherenko S, Feil B, Shah N, Mauntz W. The identification of model effective dimensions using global sensitivity analysis. Reliab Eng Syst Saf 2011;96(4):440–9. http://dx.doi.org/10.1016/j.ress.2010.11.003.

[14] Khan S, Serani A, Diez M, Kaklis P. Physics-informed feature-to-feature learning for design-space dimensionality reduction in shape optimisation. In: AIAA scitech 2021 forum. American Institute of Aeronautics and Astronautics; 2021, p. 1235. http://dx.doi.org/10.2514/6.2021-1235.

[15] Çelik C, Danışman DB, Khan S, Kaklis P. A reduced order data-driven method for resistance prediction and shape optimization of hull vane. Ocean Eng 2021;235:109406. http://dx.doi.org/10.1016/j.oceaneng.2021.109406.

[16] Sheikholeslami R, Razavi S, Gupta HV, Becker W, Haghnegahdar A. Global sensitivity analysis for high-dimensional problems: How to objectively group factors and measure robustness and convergence while reducing computational cost. Environ Model Softw 2019;111:282–99. http://dx.doi.org/10.1016/j.envsoft.2018.09.002.

[17] Yin M, Zheng X, Humphrey JD, Karniadakis GE. Non-invasive inference of thrombus material properties with physics-informed neural networks. Comput Methods Appl Mech Engrg 2021;375:113603. http://dx.doi.org/10.1016/j.cma.2020.113603.

[18] Haghighat E, Bekar AC, Madenci E, Juanes R. A nonlocal physics-informed deep learning framework using the peridynamic differential operator. Comput Methods Appl Mech Engrg 2021;385:114012. http://dx.doi.org/10.1016/j.cma.2021.114012.

[19] Krishnamurthy A, McMains S. Accurate GPU-accelerated surface integrals for moment computation. Comput Aided Des 2011;43(10):1284–95. http://dx.doi.org/10.1016/j.cad.2011.06.020.

[20] Jin P, Xie B, Xiao F. Multi-moment finite volume method for incompressible flows on unstructured moving grids and its application to fluid-rigid body interactions. Comput Struct 2019;221:91–110. http://dx.doi.org/10.1016/j.compstruc.2019.05.014.

[21] Kumar G, Taber A. An integral representation of fields with applications to finite element analysis of spatially varying materials. Comput Aided Des 2020;126:102869. http://dx.doi.org/10.1016/j.cad.2020.102869.

[22] Müller B, Kummer F, Oberlack M. Highly accurate surface and volume integration on implicit domains by means of moment-fitting. Internat J Numer Methods Engrg 2013;96(8):512–28. http://dx.doi.org/10.1002/nme.4569.

[23] Bronstein AM, Bronstein MM, Kimmel R. Numerical geometry of non-rigid shapes. Springer Science & Business Media; 2008, http://dx.doi.org/10.1007/978-0-387-73301-2.

[24] Luciano L, Hamza AB. A global geometric framework for 3D shape retrieval using deep learning. Comput. Graph. 2019;79:14–23. http://dx.doi.org/10.1016/j.cag.2018.12.003.

[25] Atrevi DF, Vivet D, Duculty F, Emile B. A very simple framework for 3D human poses estimation using a single 2D image: Comparison of geometric moments descriptors. Pattern Recognit 2017;71:389–401. http://dx.doi.org/10.1016/j.patcog.2017.06.024.

[26] Klepper O. Multivariate aspects of model uncertainty analysis: tools for sensitivity analysis and calibration. Ecol Model 1997;101(1):1–13. http://dx.doi.org/10.1016/S0304-3800(96)01922-9.

[27] Kostas K, Ginnis A, Politis C, Kaklis P. Ship-hull shape optimization with a T-spline based BEM–isogeometric solver. Comput Methods Appl Mech Engrg 2015;284:611–22. http://dx.doi.org/10.1016/j.cma.2014.10.030.

[28] Bassanini P, Bulgarelli U, Campana EF, Lalli F. The wave resistance problem in a boundary integral formulation. Surv Math Ind 1994;4:151–94.

[29] Yang L, Albregtsen F, Taxt T. Fast computation of three-dimensional geometric moments using a discrete divergence theorem and a generalization to higher dimensions. Graph Models Image Process 1997;59(2):97–108. http://dx.doi.org/10.1006/gmip.1997.0418.

[30] Saltelli A, Ratto M, Andres T, Campolongo F, Cariboni J, Gatelli D, Saisana M, Tarantola S. Global sensitivity analysis: The primer. John Wiley & Sons; 2008, http://dx.doi.org/10.1002/9780470725184.

[31] Gamboa F, Janon A, Klein T, Lagnoux A. Sensitivity indices for multivariate outputs. C R Math 2013;351(7):307–10. http://dx.doi.org/10.1016/j.crma.2013.04.016.

[32] Rajan A, Luo FJ, Kuang YC, Bai Y, Ooi MP-L. Reliability-based design optimisation of structural systems using high-order analytical moments. Struct Saf 2020;86:101970. http://dx.doi.org/10.1016/j.strusafe.2020.101970.

[33] Sheikholeslami R, Razavi S. Progressive latin hypercube sampling: An efficient approach for robust sampling-based analysis of environmental models. Environ Model Softw 2017;93:109–26. http://dx.doi.org/10.1016/j.envsoft.2017.03.010.

[34] Morio J. Global and local sensitivity analysis methods for a physical system. Eur J Phys 2011;32(6):1577. http://dx.doi.org/10.1088/0143-0807/32/6/011.

[35] Hutcheson RS, McAdams DA. A hybrid sensitivity analysis for use in early design. J Mech Des 2010;132(11):111007. http://dx.doi.org/10.1115/1.4001408.

[36] Fesanghary M, Damangir E, Soleimani I. Design optimization of shell and tube heat exchangers using global sensitivity analysis and harmony search algorithm. Appl Therm Eng 2009;29(5–6):1026–31. http://dx.doi.org/10.1016/j.applthermaleng.2008.05.018.

[37] Wu J. A new sequential space-filling sampling strategy for elementary effects-based screening method. Appl Math Model 2020;83:419–37. http://dx.doi.org/10.1016/j.apm.2020.02.032.

[38] Gong W, Duan Q, Li J, Wang C, Di Z, Ye A, Miao C, Dai Y. An intercomparison of sampling methods for uncertainty quantification of environmental dynamic models. J Environ Inf 2016;28(1):11–24. http://dx.doi.org/10.3808/jei.201500310.

[39] Storlie CB, Swiler LP, Helton JC, Sallaberry CJ. Implementation and evaluation of nonparametric regression procedures for sensitivity analysis of computationally demanding models. Reliab Eng Syst Saf 2009;94(11):1735–63. http://dx.doi.org/10.1016/j.ress.2009.05.007.

[40] Blatman G, Sudret B. Efficient computation of global sensitivity indices using sparse polynomial chaos expansions. Reliab Eng Syst Saf 2010;95(11):1216–29. http://dx.doi.org/10.1016/j.ress.2010.06.015.

[41] Cheng K, Lu Z. Adaptive sparse polynomial chaos expansions for global sensitivity analysis based on support vector regression. Comput Struct 2018;194:86–96. http://dx.doi.org/10.1016/j.compstruc.2017.09.002.
[42] Konakli K, Sudret B. Global sensitivity analysis using low-rank tensor approximations. Reliab Eng Syst Saf 2016;156:64–83. http://dx.doi.org/10.1016/j.ress.2016.07.012.
[43] Li M, Wang R-Q, Jia G. Efficient dimension reduction and surrogate-based sensitivity analysis for expensive models with high-dimensional outputs. Reliab Eng Syst Saf 2020;195:106725. http://dx.doi.org/10.1016/j.ress.2019.106725.
[44] Song J, Wei P, Valdebenito MA, Faes M, Beer M. Data-driven and active learning of variance-based sensitivity indices with Bayesian probabilistic integration. Mech Syst Signal Process 2022;163:108106. http://dx.doi.org/10.1016/j.ress.2019.106725.
[45] Pronzato L. Sensitivity analysis via Karhunen–Loève expansion of a random field model: Estimation of sobol'indices and experimental design. Reliab Eng Syst Saf 2019;187:93–109. http://dx.doi.org/10.1016/j.jcp.2018.08.036.
[46] Tarantola S, Kopustinskas V, Bolado-Lavin R, Kaliatka A, Ušpuras E, Vaišnoras M. Sensitivity analysis using contribution to sample variance plot: Application to a water hammer model. Reliab Eng Syst Saf 2012;99:62–73. http://dx.doi.org/10.1016/j.ress.2011.10.007.
[47] Milanfar P, Putinar M, Varah J, Gustafsson B, Golub GH. Shape reconstruction from moments: theory, algorithms, and applications. In: Advanced signal processing algorithms, architectures, and implementations X, Vol. 4116. International Society for Optics and Photonics; 2000, p. 406–16. http://dx.doi.org/10.1117/12.406519.
[48] Khan S, Kaklis P, Serani A, Diez M, Kostas K. Shape-supervised dimension reduction: Extracting geometry and physics associated features with geometric moments. Comput Aided Des 2022.
[49] Bui H-G, Schillinger D, Meschke G. Efficient cut-cell quadrature based on moment fitting for materially nonlinear analysis. Comput Methods Appl Mech Engrg 2020;366:113050. http://dx.doi.org/10.1016/j.cma.2020.113050.
[50] Zhang Z, Jiang W, Dolbow JE, Spencer BW. A modified moment-fitted integration scheme for X-FEM applications with history-dependent material data. Comput Mech 2018;62(2):233–52. http://dx.doi.org/10.1007/s00466-018-1544-2.
[51] Thiagarajan V, Shapiro V. Shape aware quadratures. J Comput Phys 2018;374:1239–60. http://dx.doi.org/10.1016/j.jcp.2018.05.024.
[52] Hafner C, Schumacher C, Knoop E, Auzinger T, Bickel B, Bächer M. X-CAD: optimizing CAD models with extended finite elements. ACM Trans Graph 2019;38(6):1–15. http://dx.doi.org/10.1145/3355089.3356576.
[53] Gustafsson B, He C, Milanfar P, Putinar M. Reconstructing planar domains from their moments. Inverse Problems 2000;16(4):1053. http://dx.doi.org/10.1088/0266-5611/16/4/312.
[54] Kousholt A, Schulte J. Reconstruction of convex bodies from moments. Discrete Comput Geom 2021;65(1):1–42. http://dx.doi.org/10.1007/s00454-020-00225-9.
[55] Sheynin SA, Tuzikov AV. Explicit formulae for polyhedra moments. Pattern Recognit Lett 2001;22(10):1103–9. http://dx.doi.org/10.1016/S0167-8655(01)00067-8.
[56] Xu D, Li H. Geometric moment invariants. Pattern Recognit 2008;41(1):240–9. http://dx.doi.org/10.1016/j.patcog.2007.05.001.
[57] Sobol IM. Global sensitivity indices for nonlinear mathematical models and their Monte Carlo estimates. Math Comput Simulation 2001;55(1–3):271–80. http://dx.doi.org/10.1016/S0378-4754(00)00270-6.
[58] Saltelli A, Annoni P, Azzini I, Campolongo F, Ratto M, Tarantola S. Variance based sensitivity analysis of model output. Design and estimator for the total sensitivity index. Comput Phys Comm 2010;181(2):259–70. http://dx.doi.org/10.1016/j.cpc.2009.09.018.
[59] Campbell K, McKay MD, Williams BJ. Sensitivity analysis when model outputs are functions. Reliab Eng Syst Saf 2006;91(10–11):1468–72. http://dx.doi.org/10.1016/j.ress.2005.11.049.
[60] Lamboni M, Monod H, Makowski D. Multivariate sensitivity analysis to measure global contribution of input factors in dynamic models. Reliab Eng Syst Saf 2011;96(4):450–9. http://dx.doi.org/10.1016/j.ress.2010.12.002.
[61] Garcia-Cabrejo O, Valocchi A. Global sensitivity analysis for multivariate output using polynomial chaos expansion. Reliab Eng Syst Saf 2014;126:25–36. http://dx.doi.org/10.1016/j.ress.2014.01.005.
[62] Zhang X-Y, Trame MN, Lesko LJ, Schmidt S. Sobol sensitivity analysis: a tool to guide the development and evaluation of systems pharmacology models. CPT: Pharmacomet Syst Pharmacol 2015;4(2):69–79. http://dx.doi.org/10.1002/psp4.6.
[63] Sarrazin F, Pianosi F, Wagener T. Global sensitivity analysis of environmental models: Convergence and validation. Environ Model Softw 2016;79:135–52. http://dx.doi.org/10.1016/j.envsoft.2016.02.005.
[64] Han S, Lee Y-S, Choi YB. Hydrodynamic hull form optimization using parametric models. J Mar Sci Technol 2012;17(1):1–17. http://dx.doi.org/10.1007/s00773-011-0148-8.
[65] Kim H-C. On the volumetric balanced variation of ship forms. J Ocean Eng Technol 2013;27(2):1–7.
[66] Lackenby H. On the systematic geometrical variation of ship forms. Trans TINA 1950;92:289–315.
[67] Abt C, Harries S. A new approach to integration of CAD and CFD for naval architects. In: Sixth international conference on computer applications and information technology in the maritime industries (COMPIT), Cortona. 2007, p. 467–79.
[68] Birk L, Wegemt, School WS. Optimistic: optimization in marine design. Mensch & Buch Verlag; 2003.
[69] Tuck EO. Shallow-water flows past slender bodies. J Fluid Mech 1966;26(1):81–95. http://dx.doi.org/10.1017/S0022112066001101.
[70] Tuck EO. Wave resistance of thin ships and catamarans. Applied mathematics report, internal report T8701, University of Adelaide; 1987.
[71] Wehausen JV. The wave resistance of ships. In: Advances in applied mechanics, Vol. 13. Elsevier; 1973, p. 93–245. http://dx.doi.org/10.1016/S0065-2156(08)70144-3.
[72] Khan S, Gunpinar E, Dogan KM. A novel design framework for generation and parametric modification of yacht hull surfaces. Ocean Eng 2017;136:243–59. http://dx.doi.org/10.1016/j.oceaneng.2017.03.013.
[73] Hughes TJ, Cottrell JA, Bazilevs Y. Isogeometric analysis: CAD, finite elements, NURBS, exact geometry and mesh refinement. Comput Methods Appl Mech Engrg 2005;194(39–41):4135–95. http://dx.doi.org/10.1016/j.cma.2004.10.008.
[74] Fox RO, Laurent F, Vié A. Conditional hyperbolic quadrature method of moments for kinetic equations. J Comput Phys 2018;365:269–93. http://dx.doi.org/10.1016/j.jcp.2011.07.020.
[75] Khan S, Gunpinar E. Sampling CAD models via an extended teaching–learning-based optimization technique. Comput Aided Des 2018;100:52–67. http://dx.doi.org/10.1016/j.cad.2018.03.003.
[76] Kalogerakis E, Averkiou M, Maji S, Chaudhuri S. 3D shape segmentation with projective convolutional networks. In: Proceedings of the IEEE conference on computer vision and pattern recognition; 2017, p. 3779–88.
[77] Rao R. Jaya: A simple and new optimization algorithm for solving constrained and unconstrained optimization problems. Int J Ind Eng Comput 2016;7(1):19–34. http://dx.doi.org/10.5267/j.ijiec.2015.8.004.
[78] Khan S, Gunpinar E, Sener B. GenYacht: An interactive generative design system for computer-aided yacht hull design. Ocean Eng 2019;191:106462. http://dx.doi.org/10.1016/j.oceaneng.2019.106462.
[79] Khan S, Gunpinar E, Moriguchi M, Suzuki H. Evolving a psycho-physical distance metric for generative design exploration of diverse shapes. J Mech Des 2019;141(11). http://dx.doi.org/10.1115/1.4043678.